Università di Trieste

LAUREA MAGISTRALE IN GEOSCIENZE SM62A

Percorso Esplorazione Geologica

Anno accademico 2026 - 2027

Geologia Marina 953SM

Modulo 1.1 Oceani. Morfologia, struttura ed evoluzione

Docente

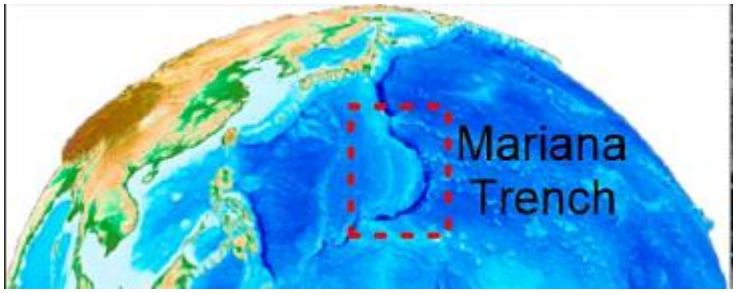
Laura De Santis

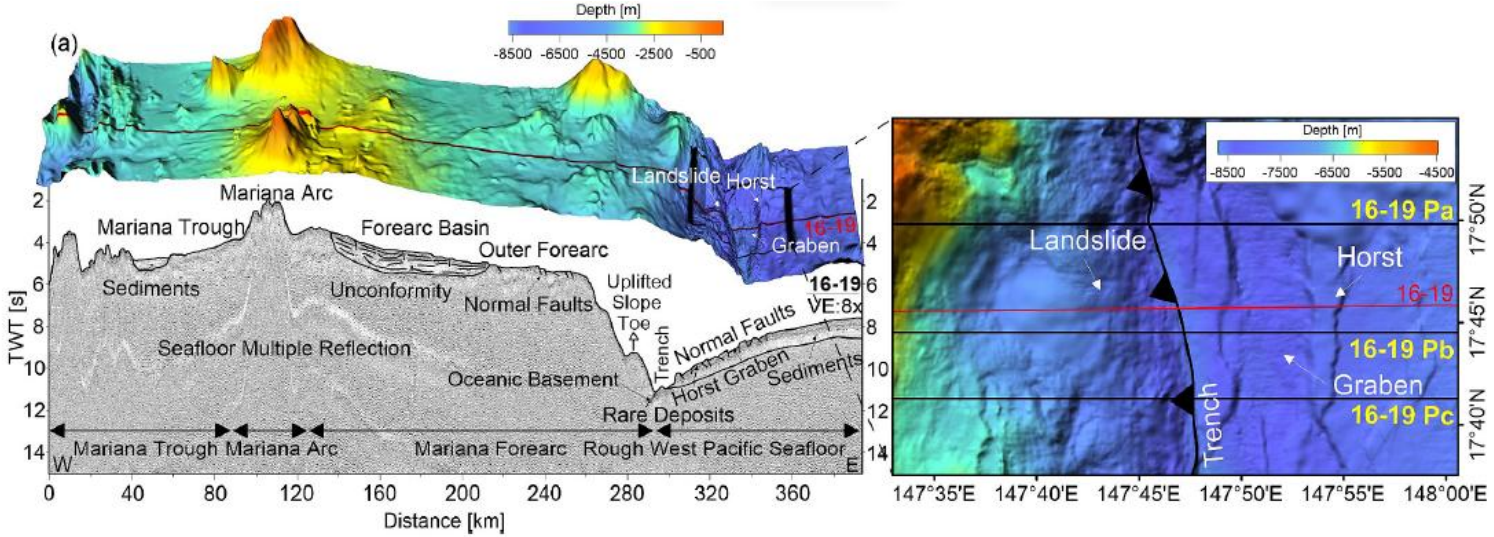
(con contributo di Martina Busetti)

Examples of data used to understand the morphology and the geological structure of the oceans

Subduction erosion (Miller, 1970; Murauchi, 1971) factors:

- thinner trench sediments (<1 km),
- faster plate convergence rate (>60 mm/yr),
- steeper inner-trench wall,
- high-relief topography on the subducting plate
- subduction of submarine relief (e.g., seamounts and ridges)





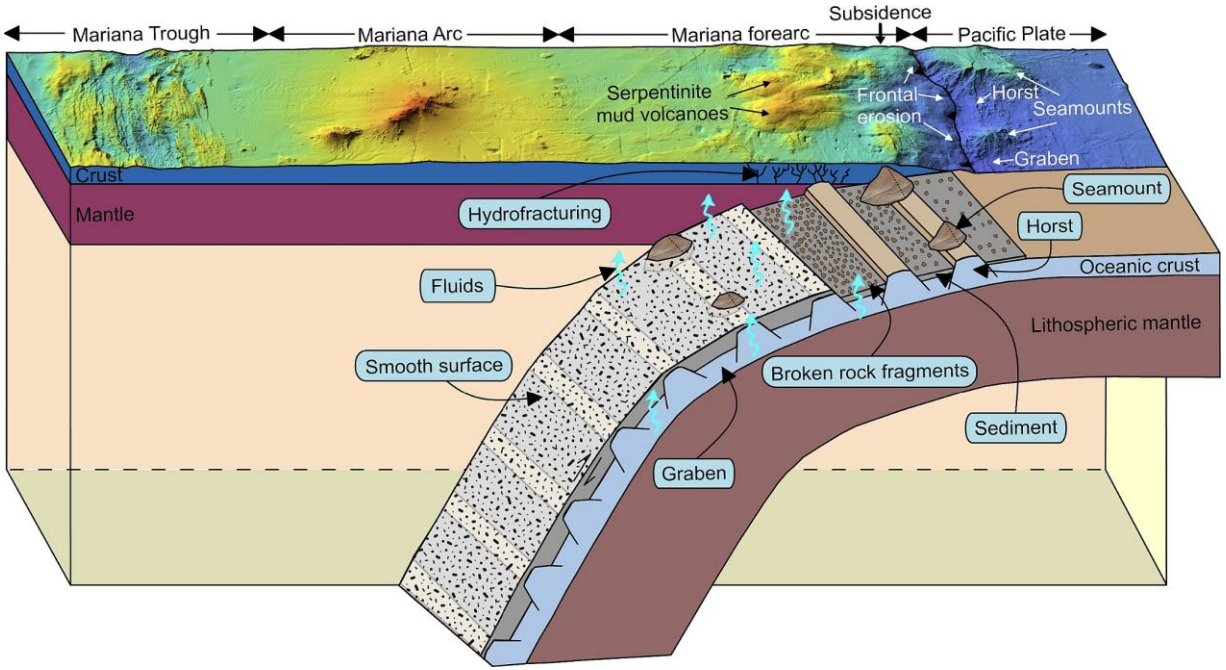
small frontal prism and the forearc crust is positioned very close to the trench axis

bending stresses are accommodated by normal faults, and horst and graben => when enter the subduction zone they erode the accretionary wedge and base of the overriding plate

Liu et al., 2024. Geomorphology and mechanisms of subduction erosion in the sediment-starved Mariana convergent margin. *Geomorphology 454 (2024) 109161*

fluids rising with serpentinite mudflows and melting flux are derived from dehydration of subducting oceanic lithosphere => fluids (mainly water) might substantially affect the subduction erosion of the Mariana margin

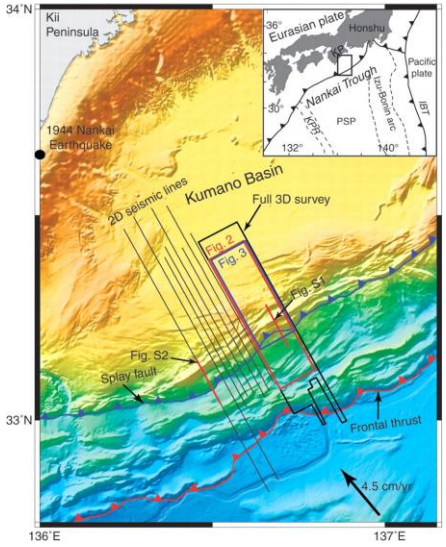
Dewatering elevates the pore pressure in the interplate interval, and allows a large volume of fluid into the bottom of the overriding plate, eventually triggering a special type of basal erosion known as **hydrofracturing**

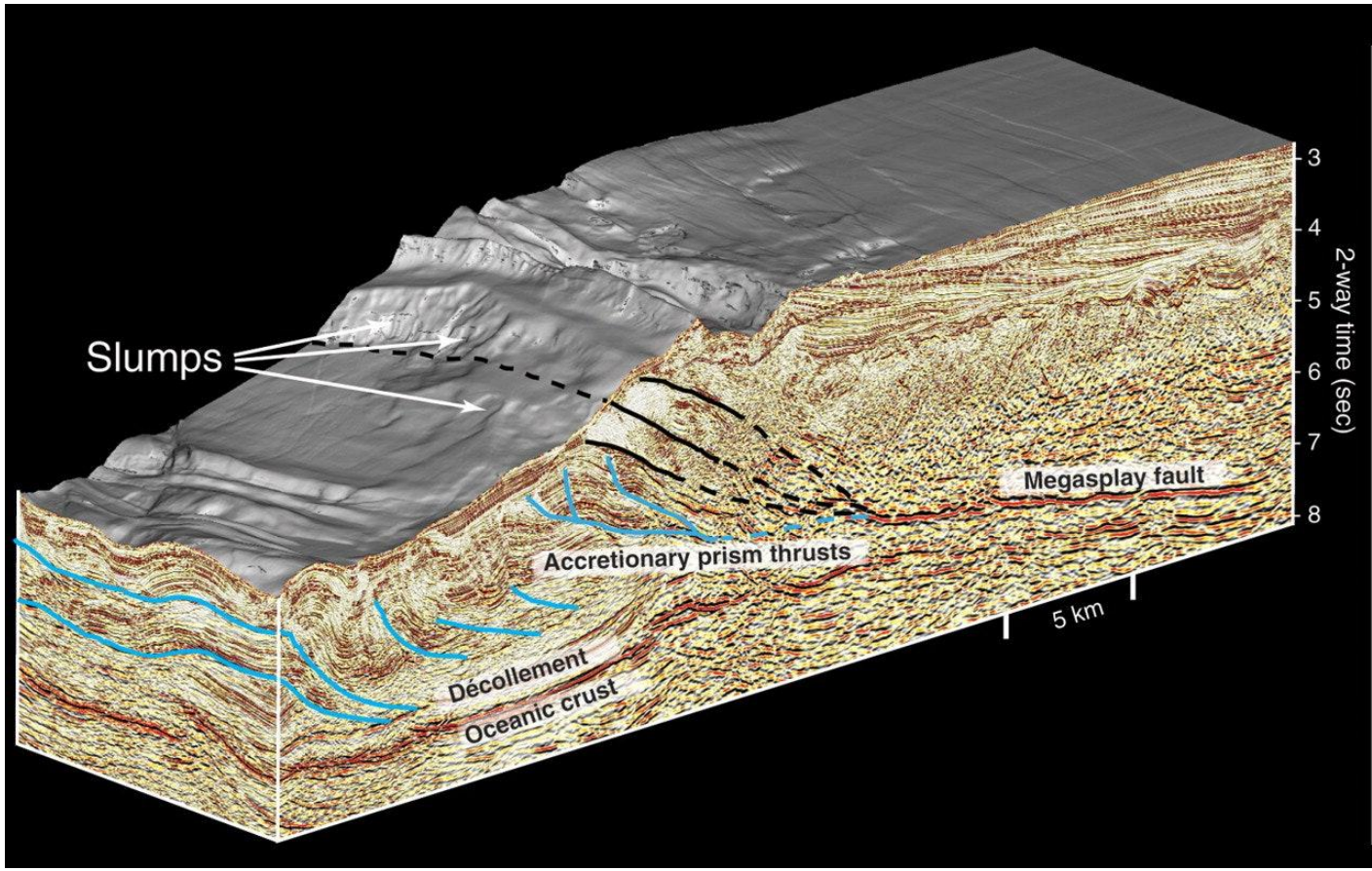


Liu et al., 2024. Geomorphology and mechanisms of subduction erosion in the sediment-starved Mariana convergent margin. *Geomorphology 454 (2024) 109161*

The thrust geometry and evidence of **large-scale slumping** of surficial sediments show that the fault is active and that the activity has evolved toward the landward direction with time, contrary to the usual seaward progression of accretionary thrusts.

The megasplay fault has progressively steepened, substantially increasing the potential for vertical uplift of the sea floor with slip





Moore et al., 2007, Three-dimensional splay fault geometry and implications for tsunami generation: Science, v. 318, p. 1128-1131.
DOI: 10.1126/science.1147195

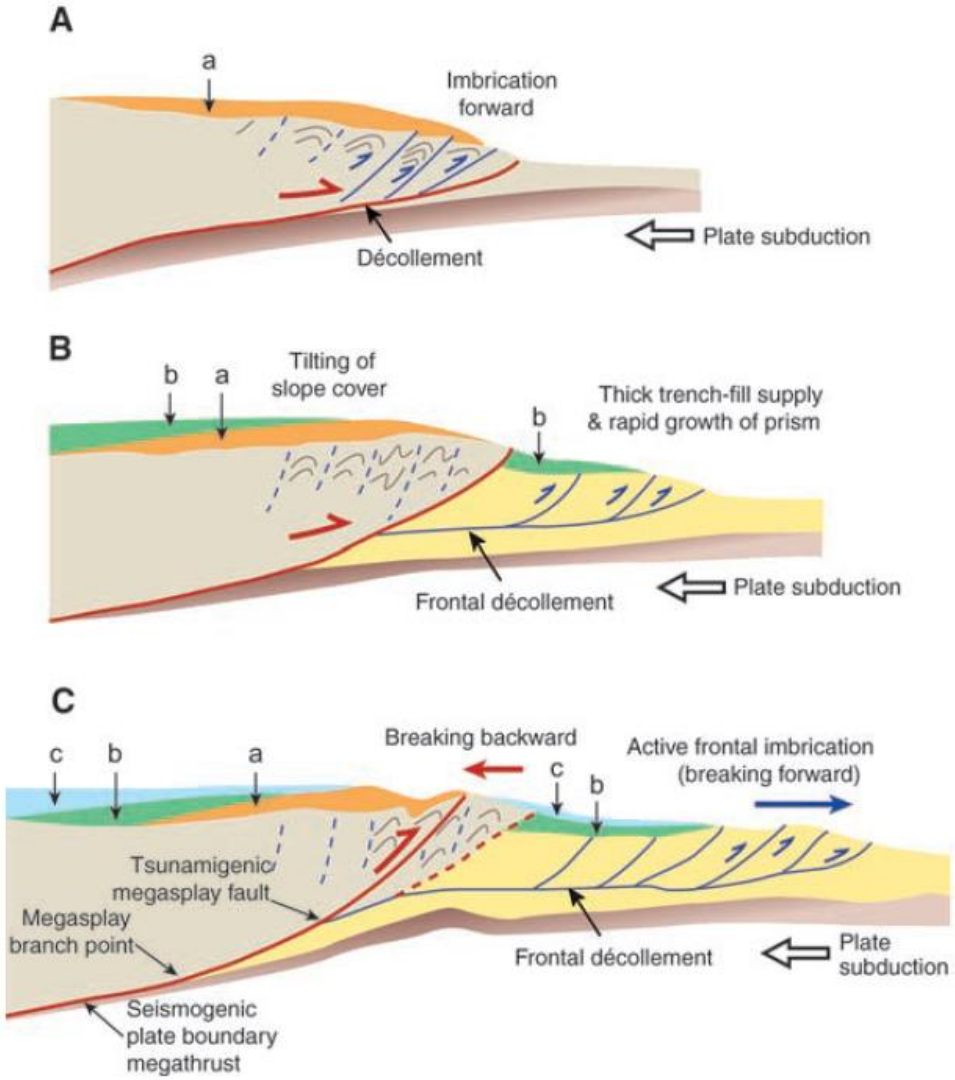
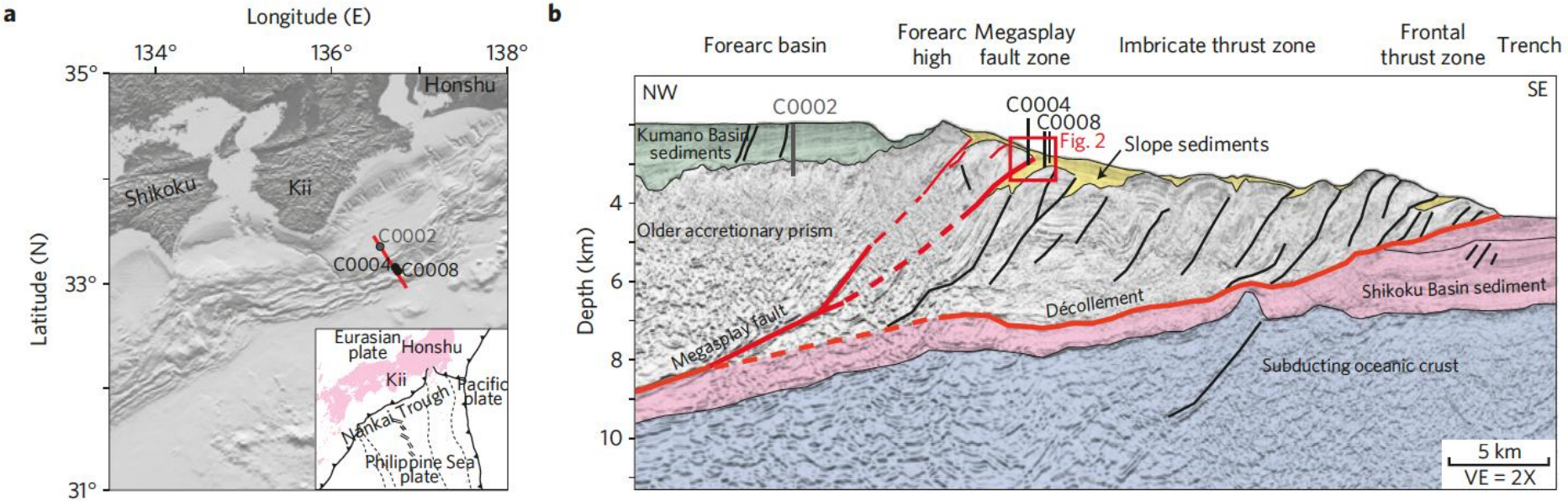


Fig. 4. (**A** to **C**) Summary diagram showing the development of the Nankai accretionary prism in the Kumano Basin area. After "normal" in-sequence thrusting and building of an accretionary prism, an out-of-sequence (splay) fault system broke through at the back of the prism. a, b, and c refer to sequential sedimentary sequences.

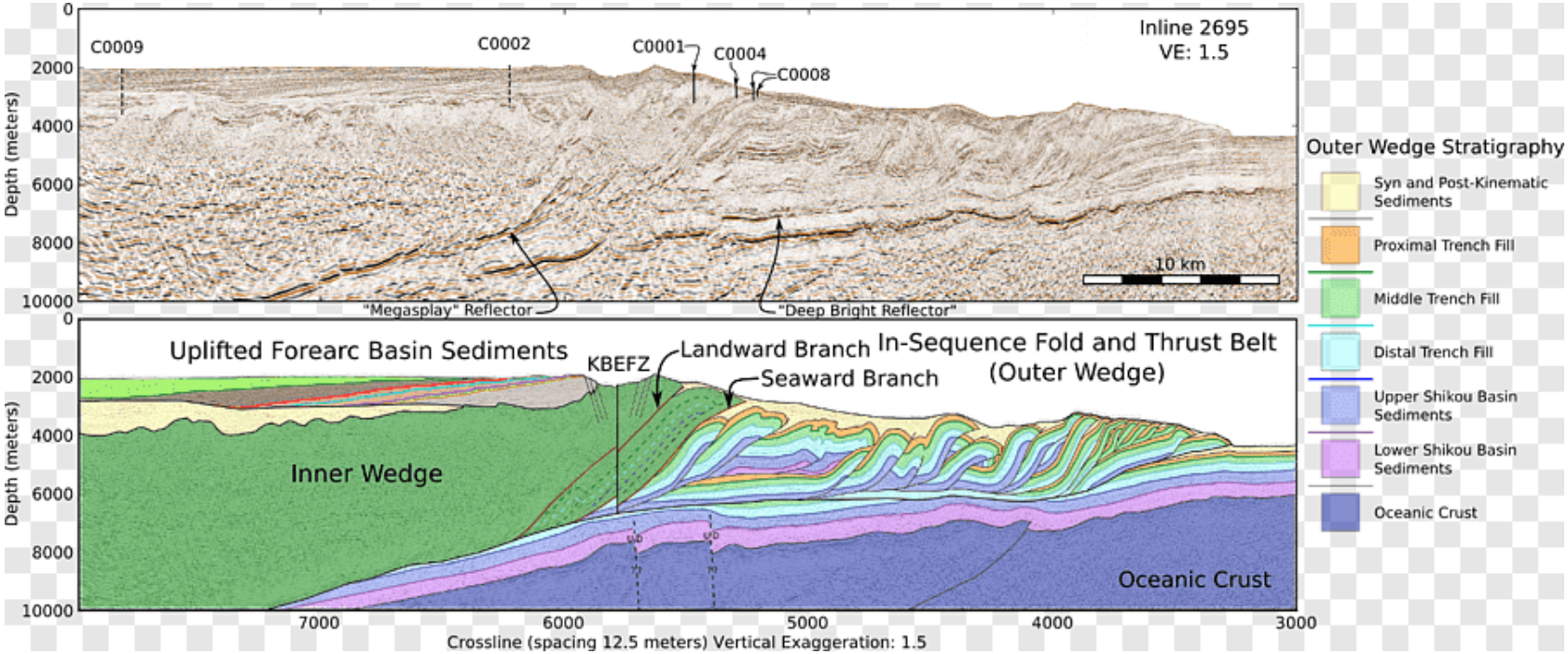
Moore et al., 2007, Three-dimensional splay fault geometry and implications for tsunami generation: Science, v. 318, p. 1128-1131. DOI: 10.1126/science.1147195

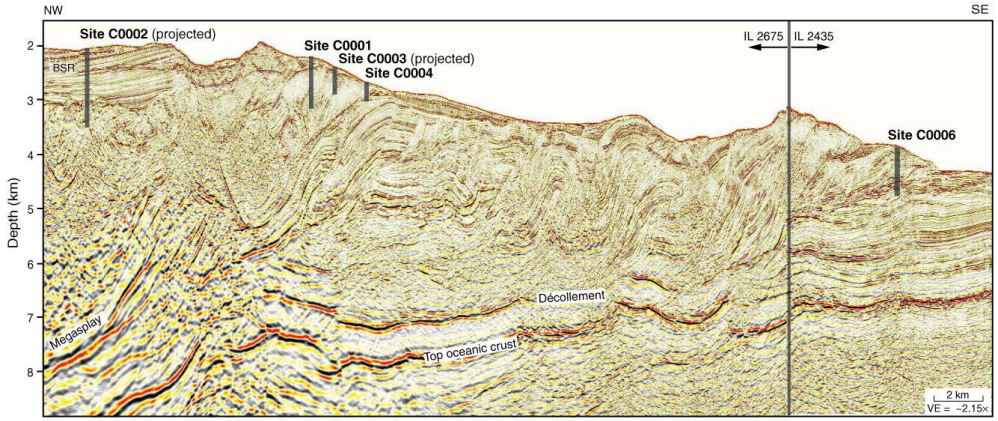


Strasser et al., 2009. Origin and evolution of a splay fault in the Nankai accretionary wedge. Nature Geoscience,

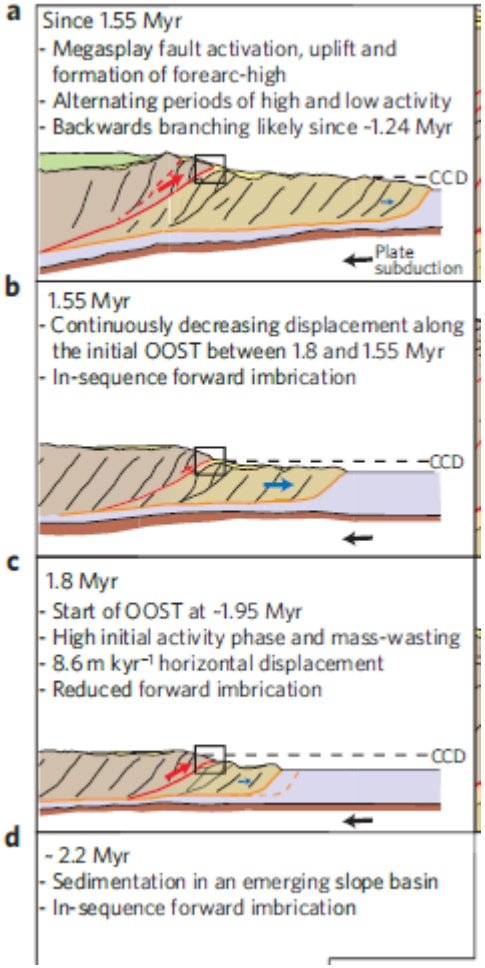
MODERN SUBDUCTION ZONES

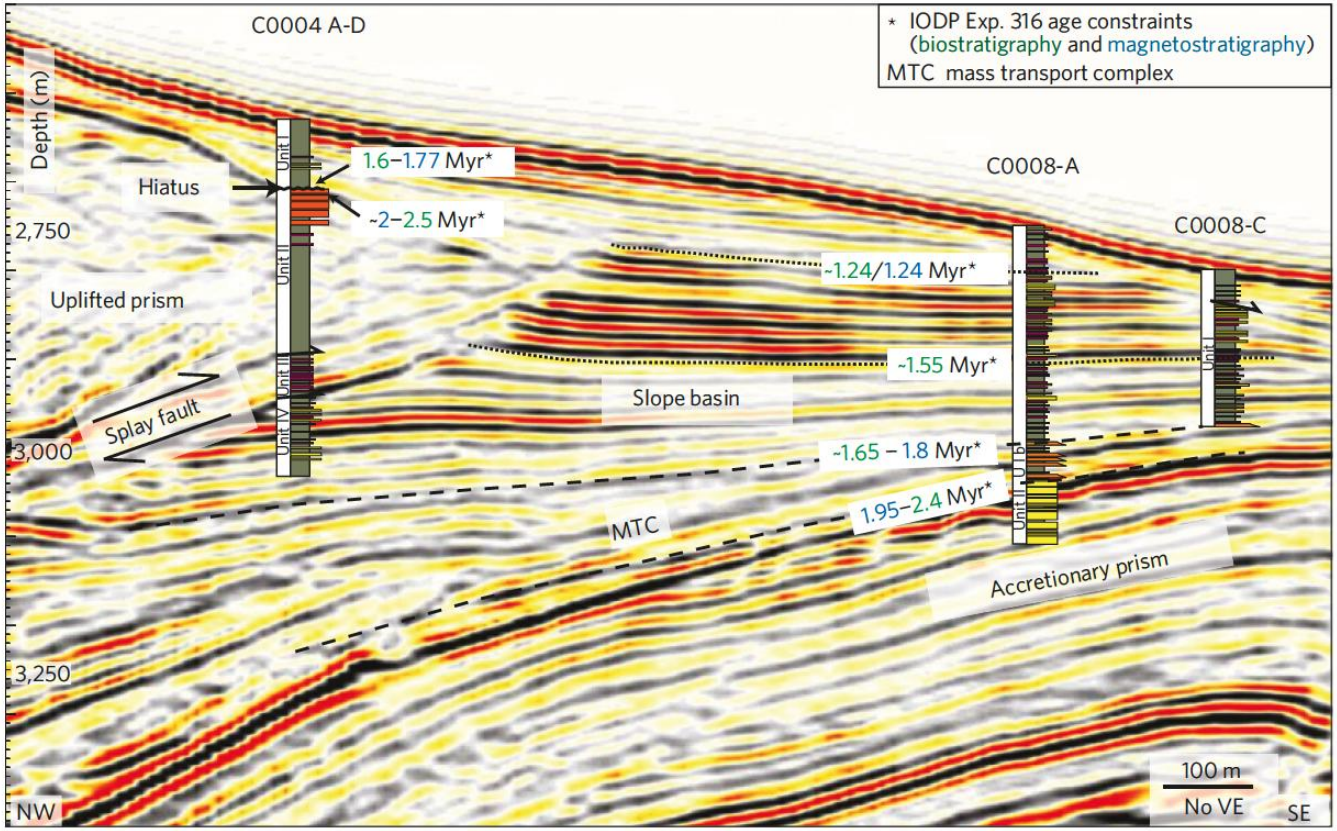
IODP Exp 315 NanTroSEIZE



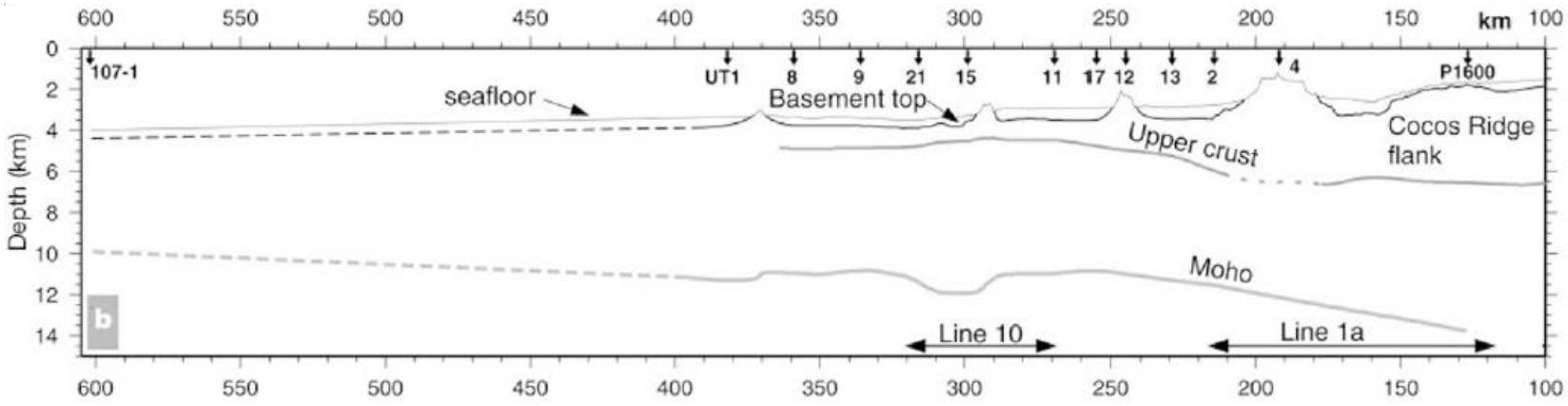


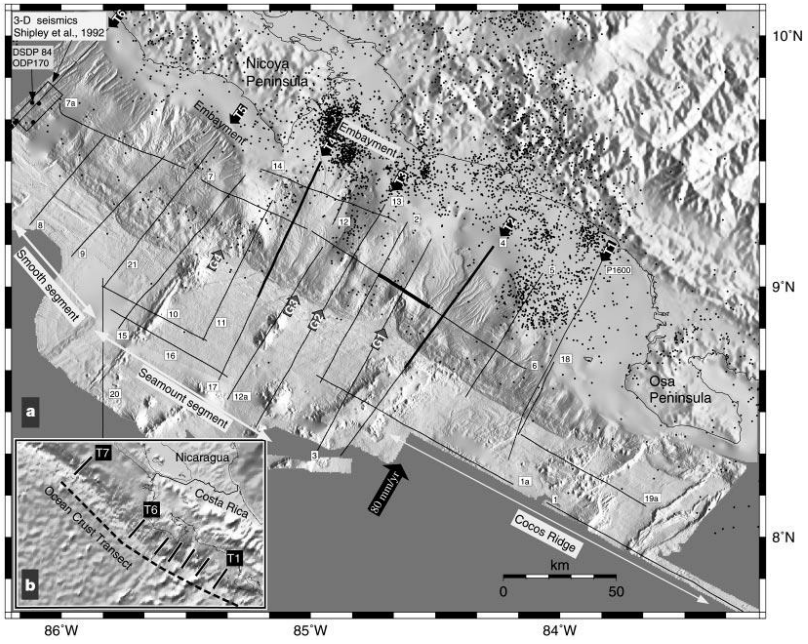
the splay fault cutting this wedge initiated 1:95 Million years (Myr) ago
the fault resumed about 1.55 Myr ago.





Strasser et al., 2009. Origin and evolution of a splay fault in the Nankai accretionary wedge. Nature Geoscience,



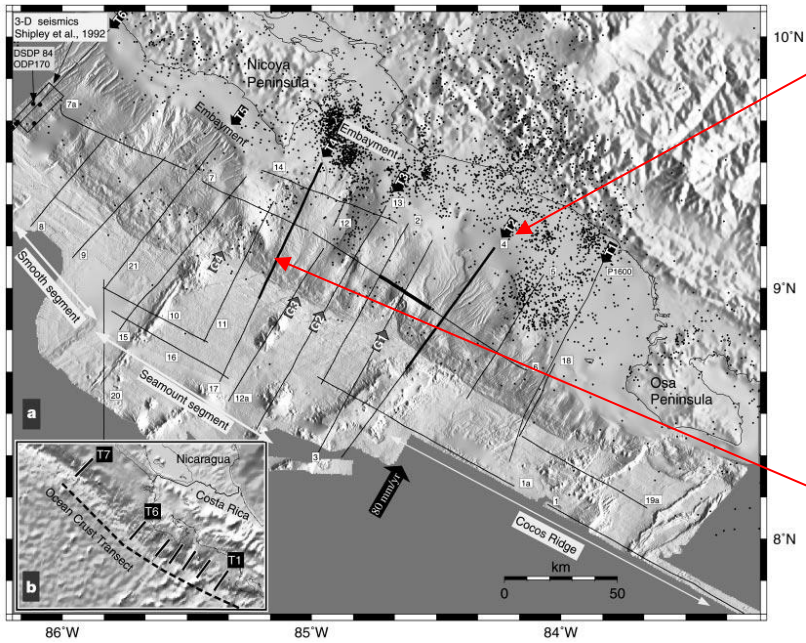


- erosion by seamount tunnelling
- removal of large rock lenses of a distending upper plate.

Ranero and VonHuenen, 2000. Subduction erosion along the Middle America convergent margin. Nature 404

high-amplitude reflections define the plate interface of the Costa Rica-Nicaragua margin at depths corresponding to calculated temperatures of 60–150◦ and are due to free water along the decollement

margin wedge is .6±8 km thick its top is smooth, only cut by normal faulting



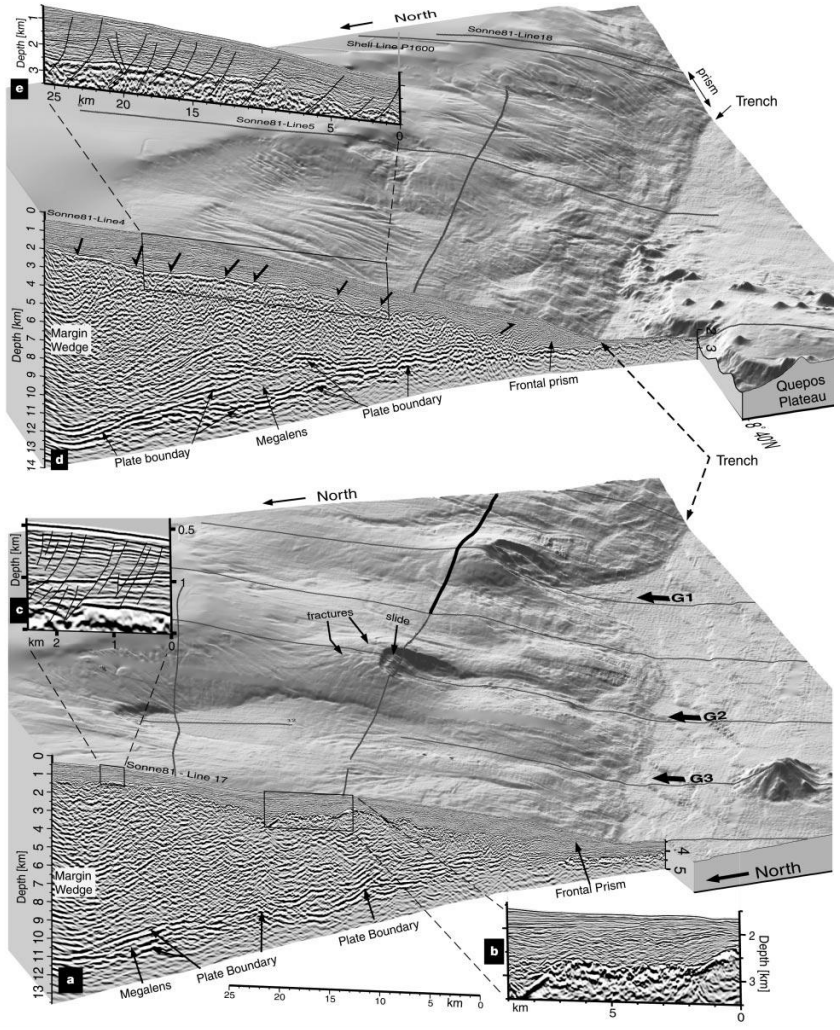
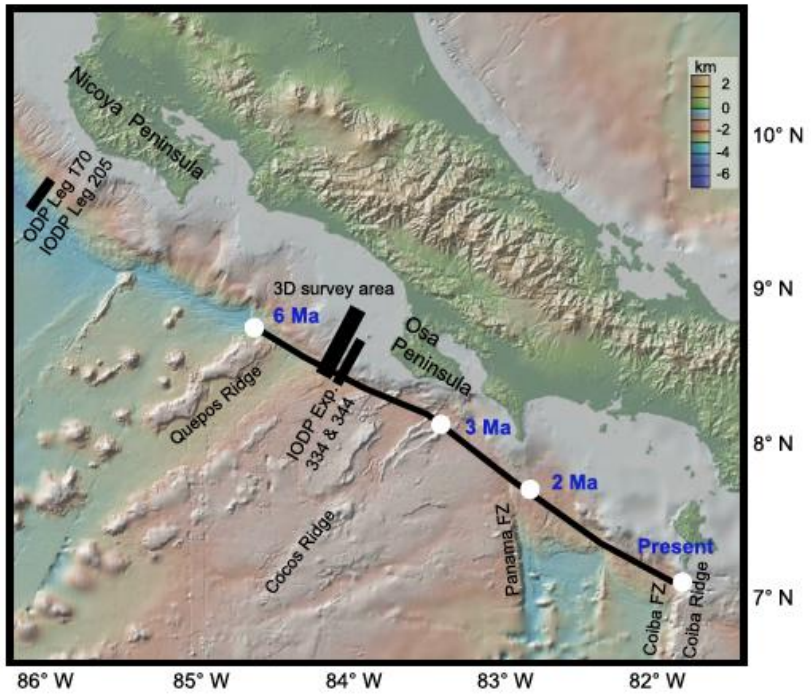
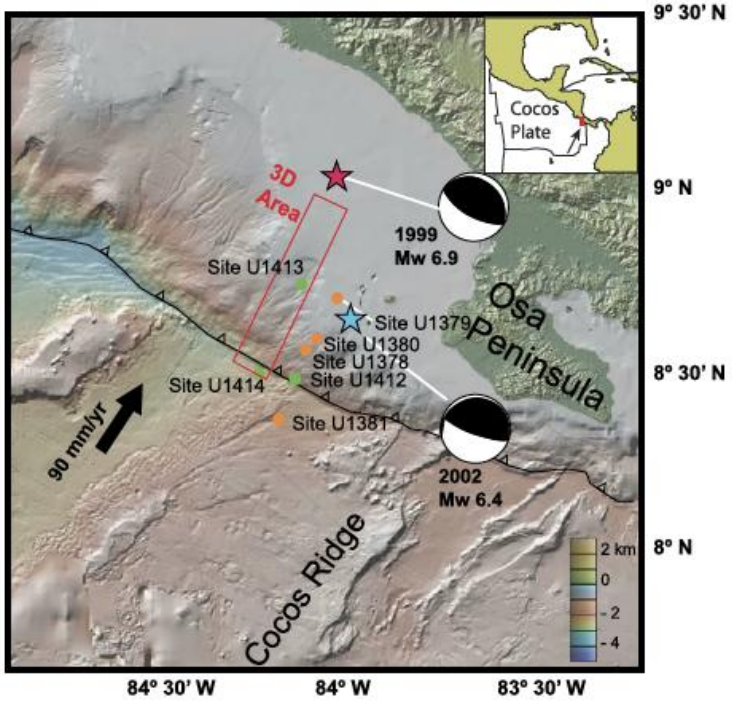


plate-boundary reflections bifurcate and surround a rock megalens

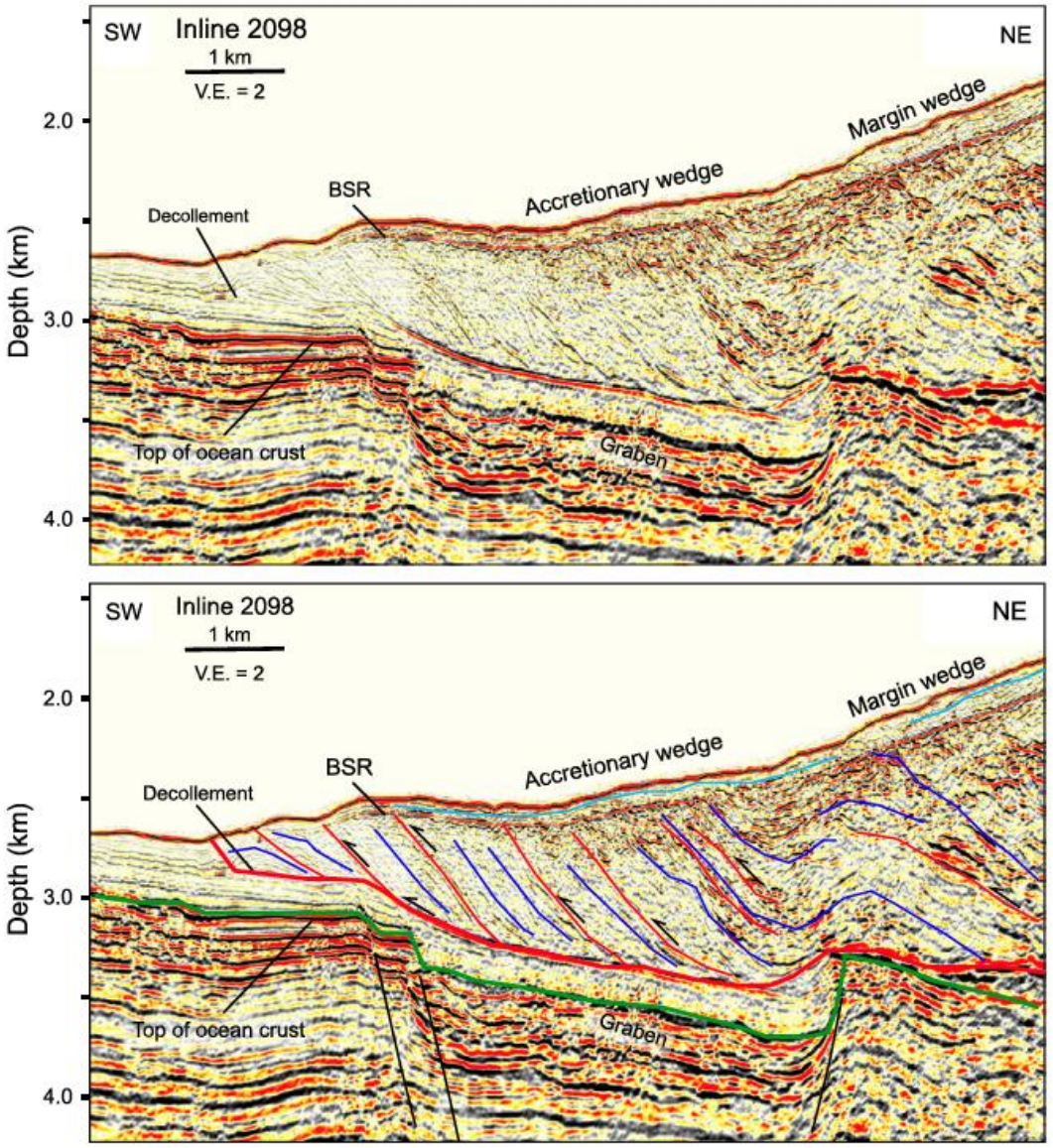
underthrusting of seamounts

Ranero and VonHuenen, 2000. Subduction erosion along the Middle America convergent margin. Nature 404



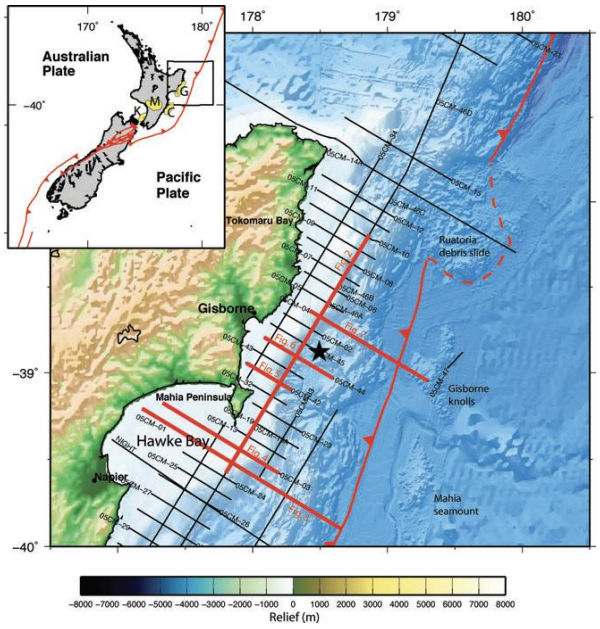


Bangs et al., 2016. A recent phase of accretion along the southern Costa Rican subduction zone Earth and Planetary Science Letters, 443, 204-215

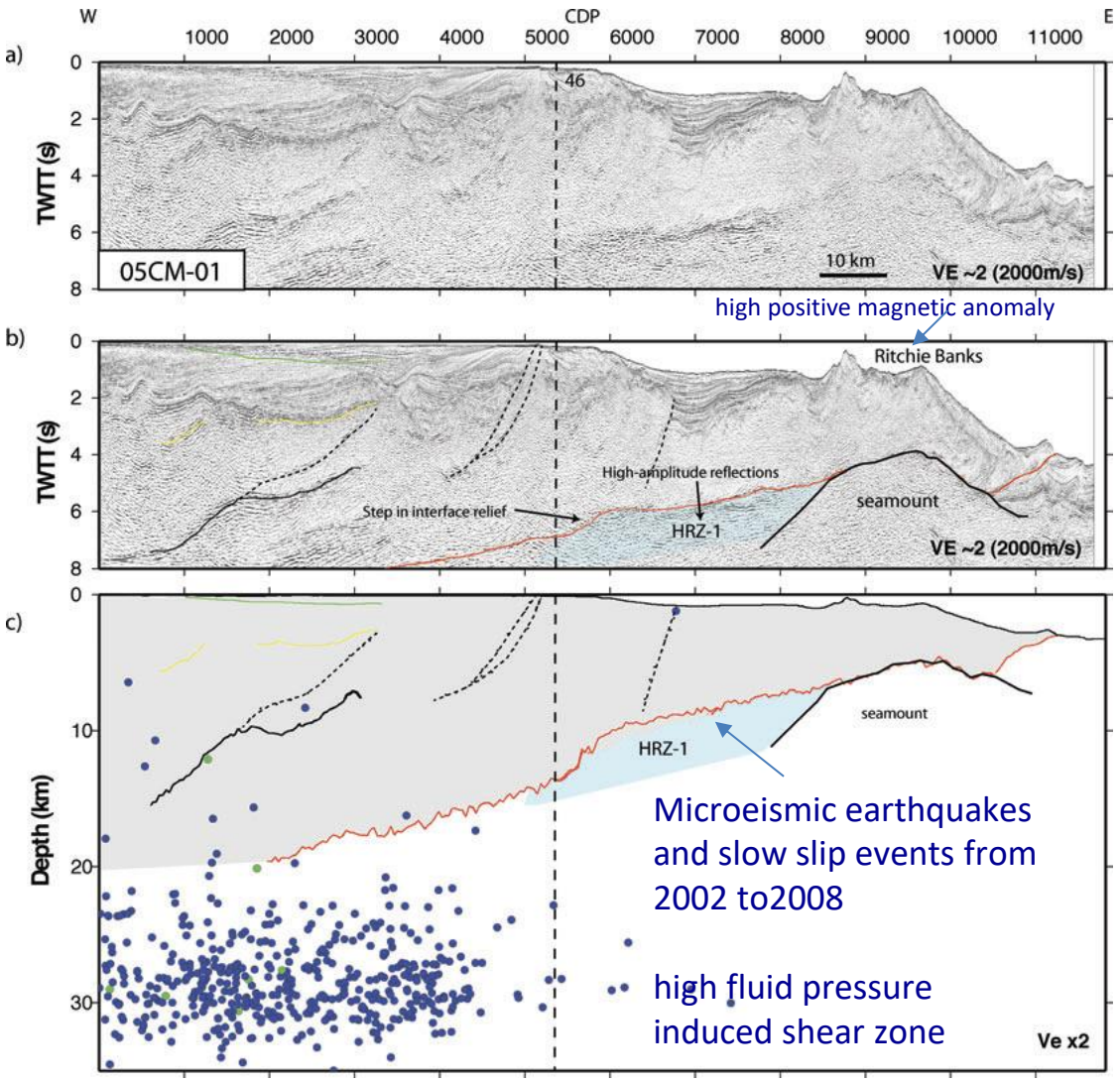


Bangs et al., 2016. A recent phase of accretion along the southern Costa Rican subduction zone Earth and Planetary Science Letters, 443, 204-215

potential fluid flow
concentration effects
leading to overpressure



HRZ: high-amplitude interface reflectivity are interpreted to be the result of fluid-rich sediments that have been entrained with subducting seamounts



Bell et al., 2010Seismic reflection character of the Hikurangi subduction interface New Zealand, in the region of repeated Gisborne slow slip events Geophys. J. Int. 180, 34–48

Inheritance

Most present-day rifted margins were built upon earlier continental collision zones

Faults

Normal faults facilitate extension and eventual rupture of continental crust

Stratigraphy

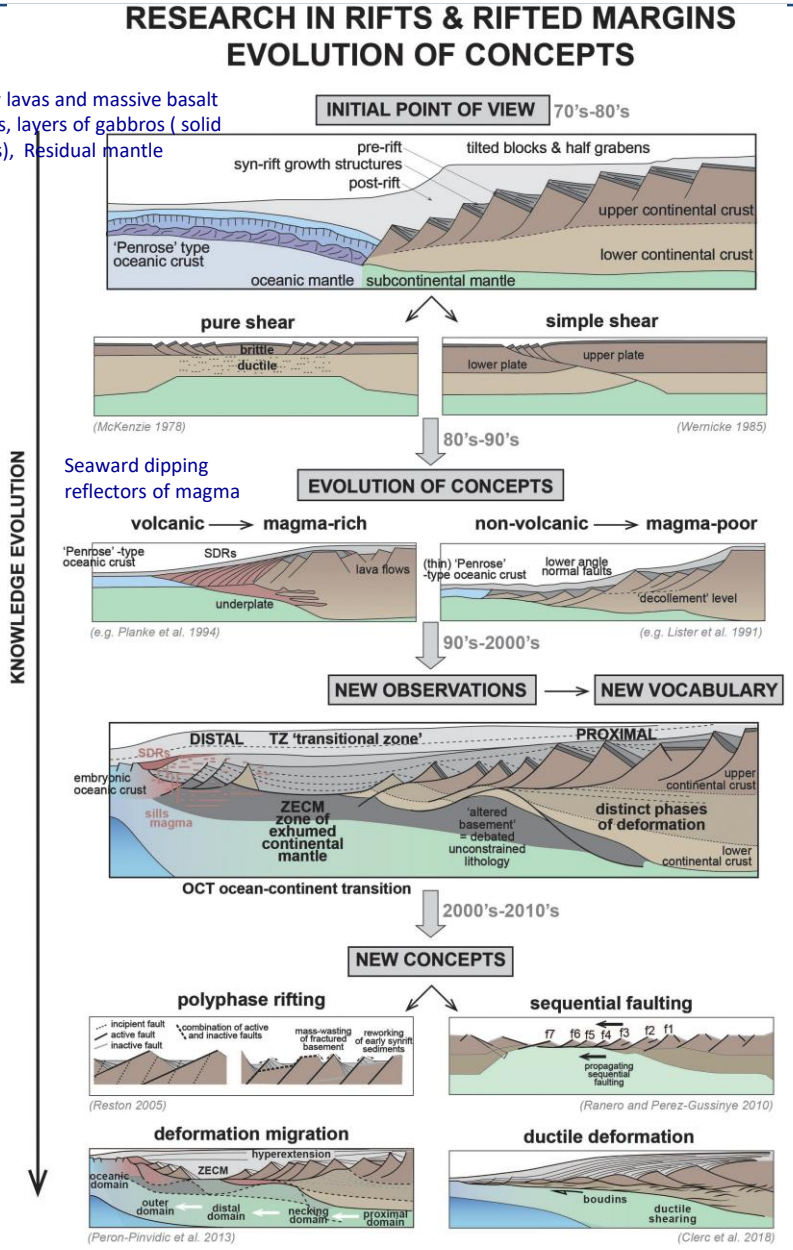
polyphase, re-activation and de-activation of faults segments imply specific depositional environments for the sediments (good age model is needed).

Mantle

plays a major role in rifted margin evolution, influencing the structural, rheological, and magmatic activities

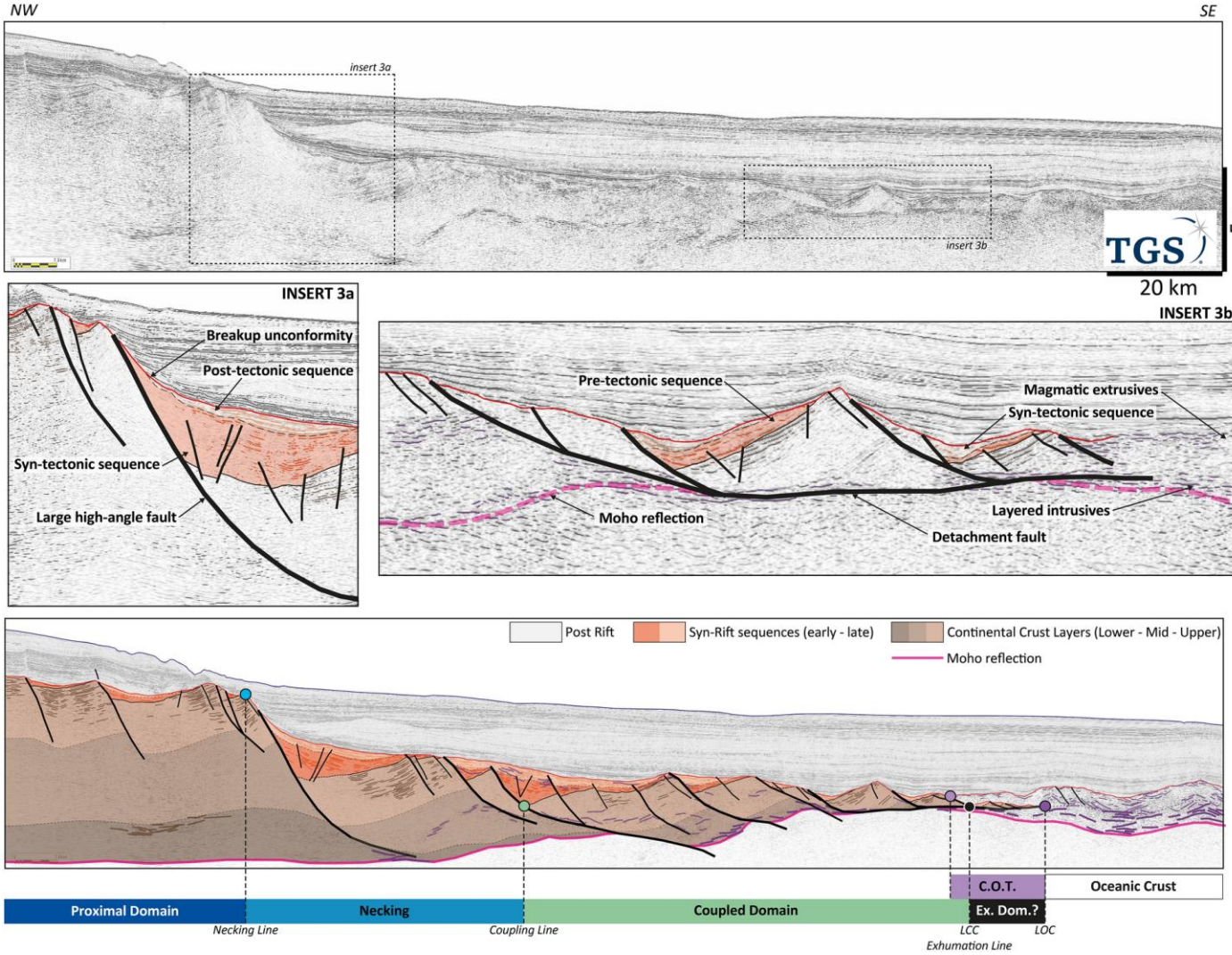
Rheology

At magma-poor margins key issues relate to the role of different rheologies (brittle vs. ductile)



Peron-Pinvidic et al., 2019. Rifted Margins: State of the Art and Future Challenges. Front. Earth Sci. 7:218.

Rifted margins classification based on mechanical behavior and magmatic production



Top basement and a seismic Moho converging oceanward, indicating an effective thinning of the continental crust

The Necking Line: the footwall cut of first large trans-crustal fault, coupling down to the mantle

Coupling Domain presents several low-angle normal faults merging into a single detachment (both Limit of Continental Crust (LCC) and Exhumation Line (EL)

breakup unconformity (Top Rift).

Sapin et al., 2021. Rifted margins classification and forcing parameters. Scientific Reports, 8199.

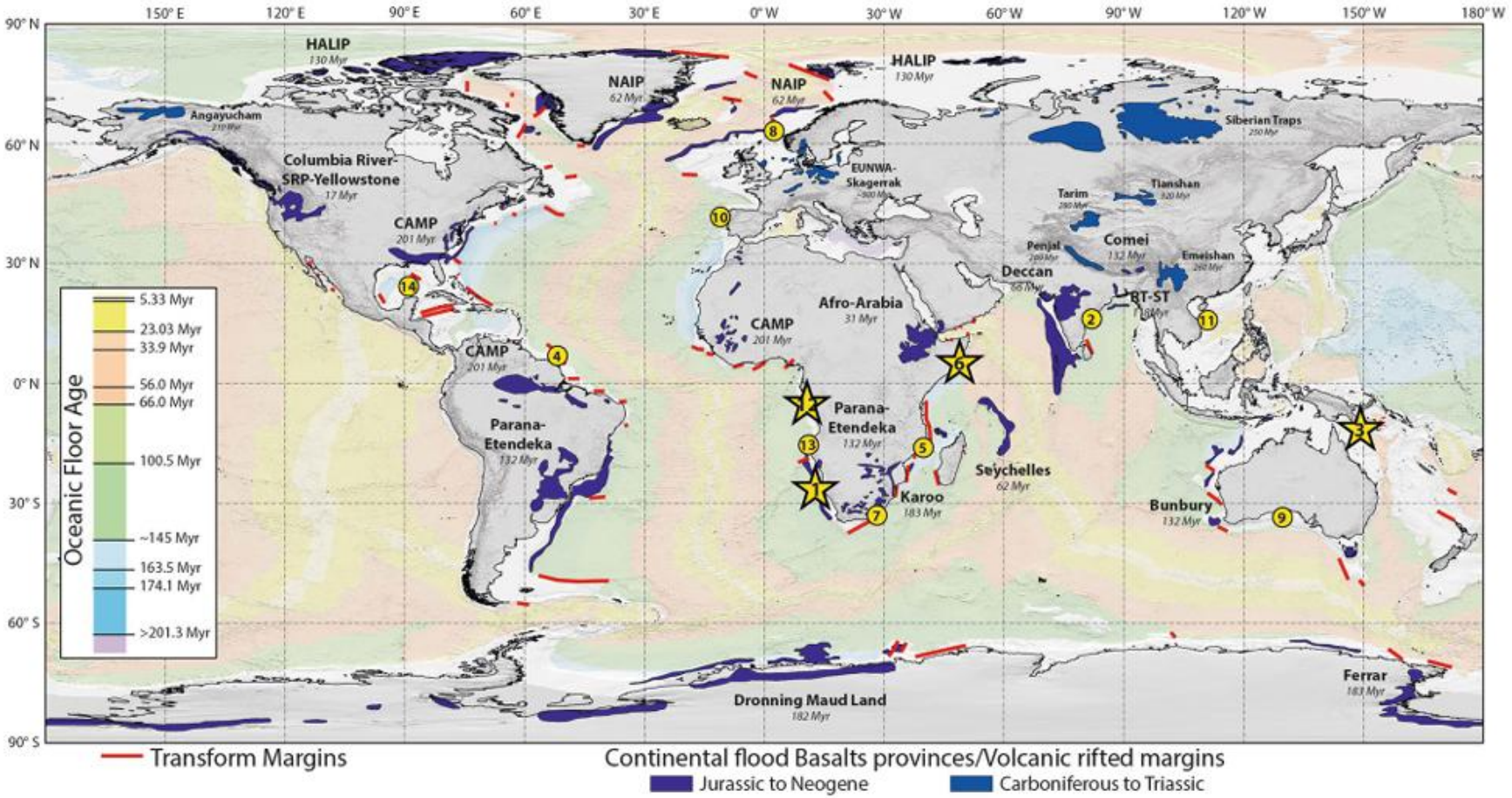
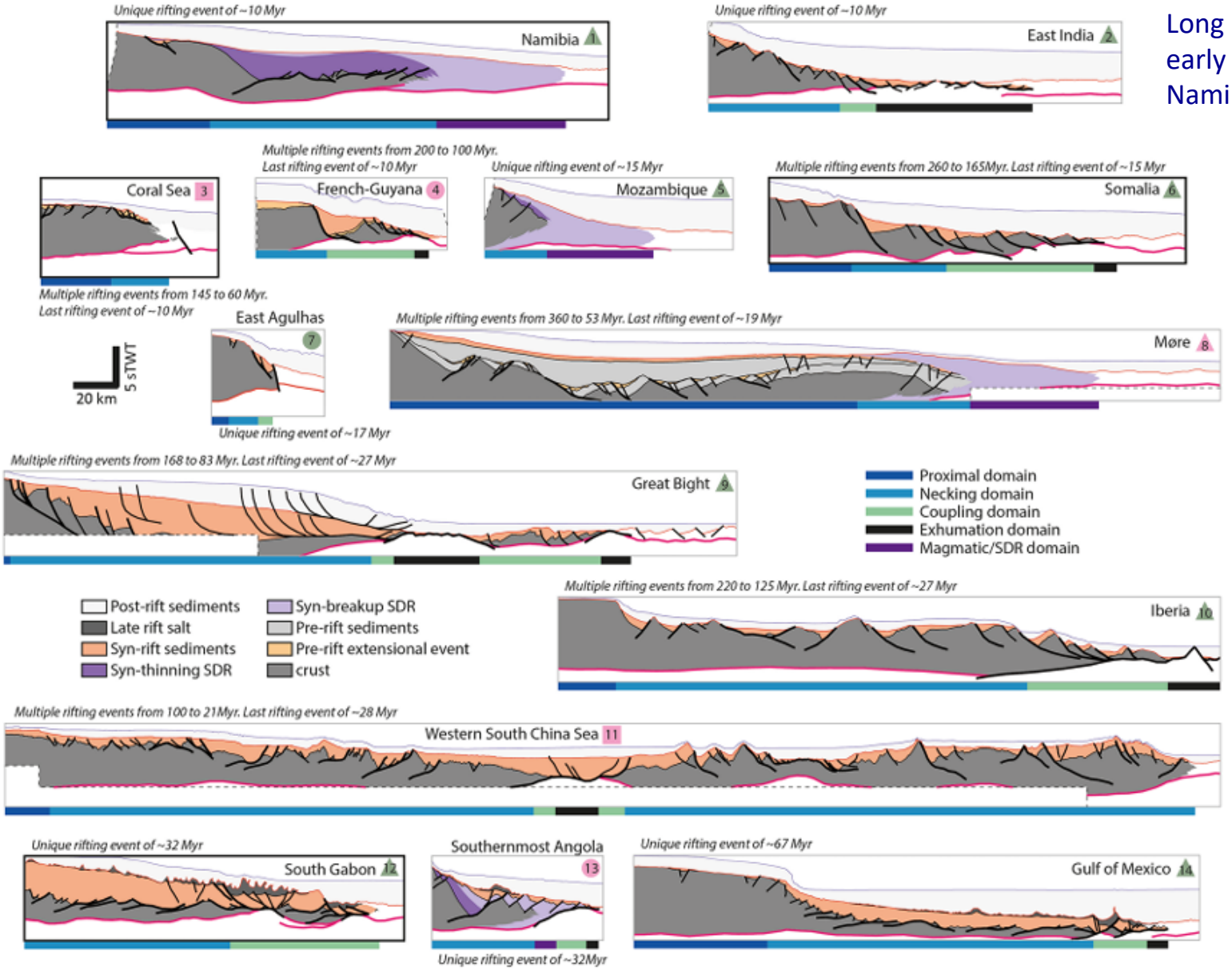


Figure 2. Location of the examples and case studies. The examples shown in Fig. 1 are located on the world map with the oceanic floor age from Müller et al.[133]. The main case studies are emphasized with stars. The main transform margins[134] and continental flood basalts provinces/volcanic rifted margins (modified from Bryan and Ferrari[135]) are also shown.

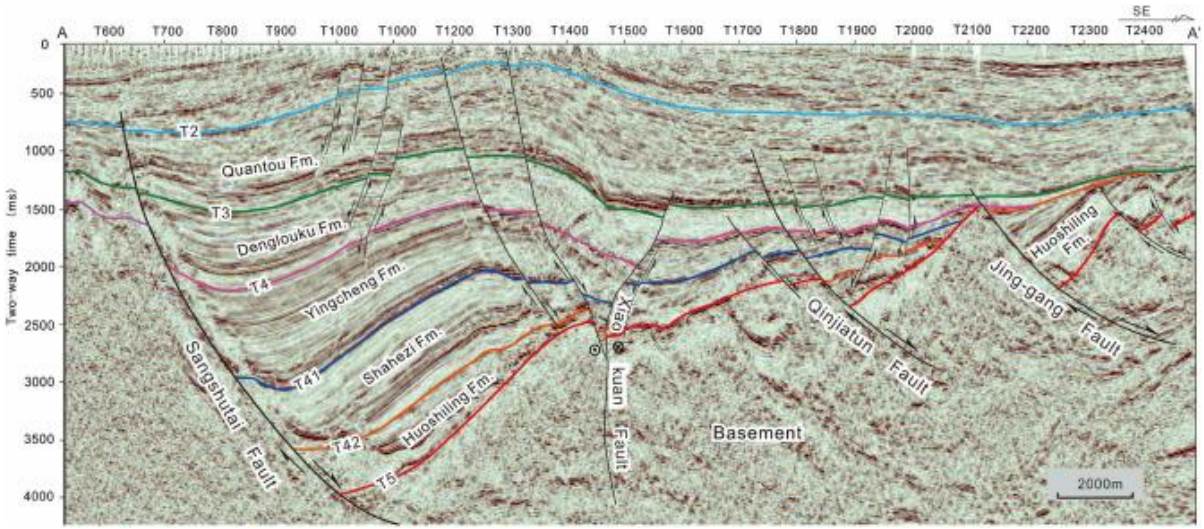


Long necking taper and early magmatic input: South Namibia

Localized deformation, narrow necking and late magmatic breakup: Somalia

Long necking taper, multiple core complexes and late magmatic breakup: South Gabon

Rifted margins

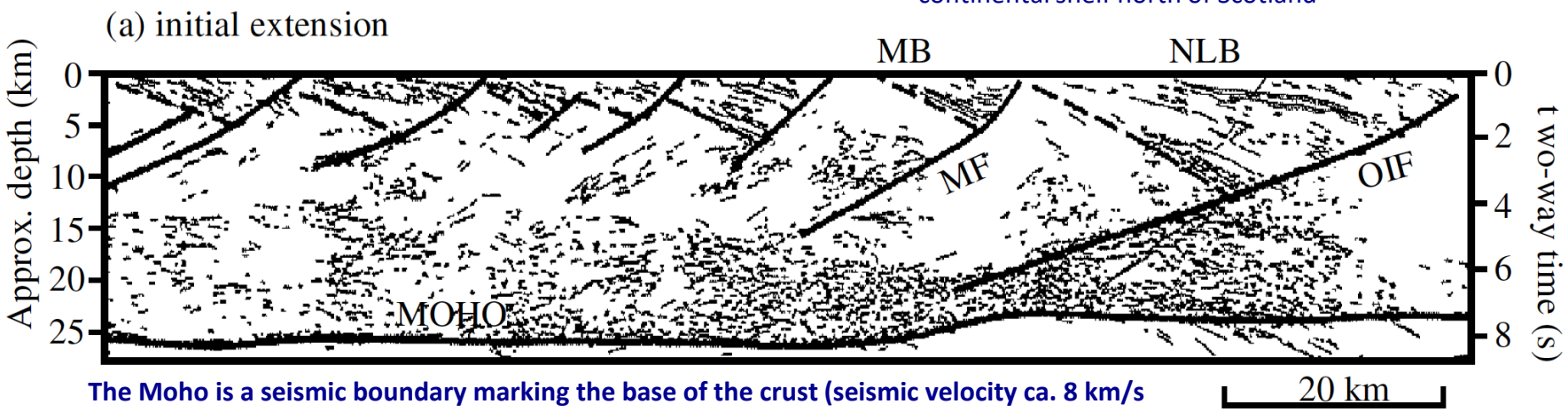


Yang et al., 2021. Tectonic-sedimentary evolution of a continental rift basin: A case study of the Early Cretaceous Changling and Lishu fault depressions, southern Songliao Basin, China. Marine and Petroleum Geology, Volume 128, 105068

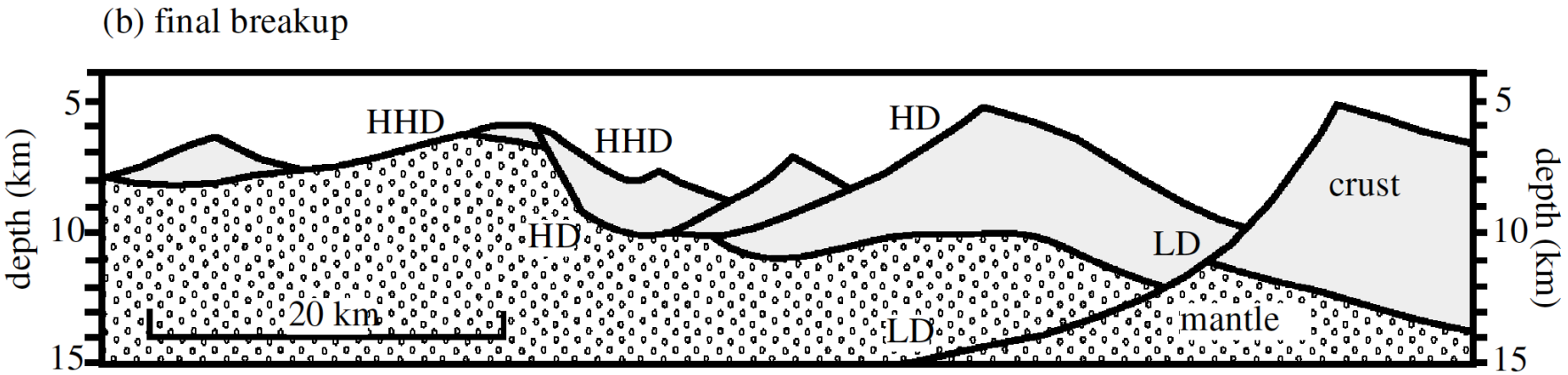
LITHOSPHERIC STRUCTURE INDICATORS

Structure from seismic reflections/refraction

continental shelf north of Scotland



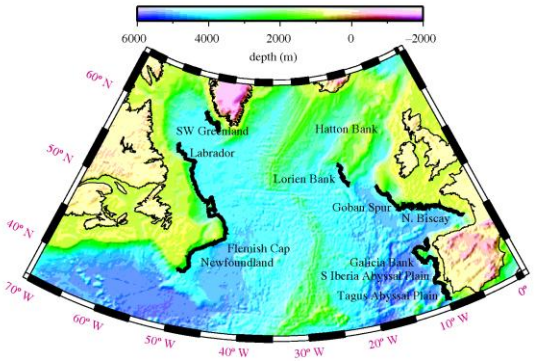
The Moho is a seismic boundary marking the base of the crust (seismic velocity ca. 8 km/s



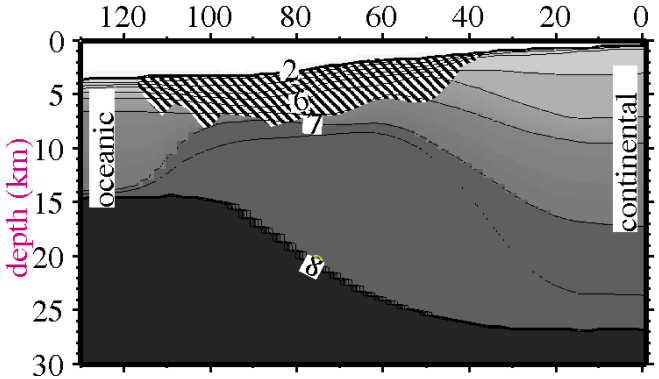
Minshull, 2002. The break-up of continents and the formation of new ocean basins. *Phil. Trans. R. Soc. Lond. A* 2002 **360**, 2839-2852

LITHOSPHERIC STRUCTURE INDICATORS

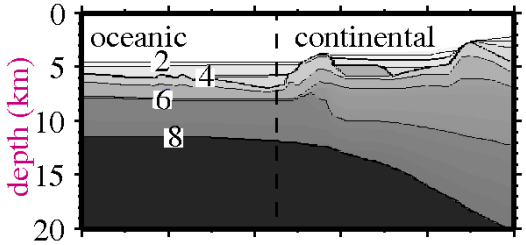
Seismic Velocity (Vp, Vs)

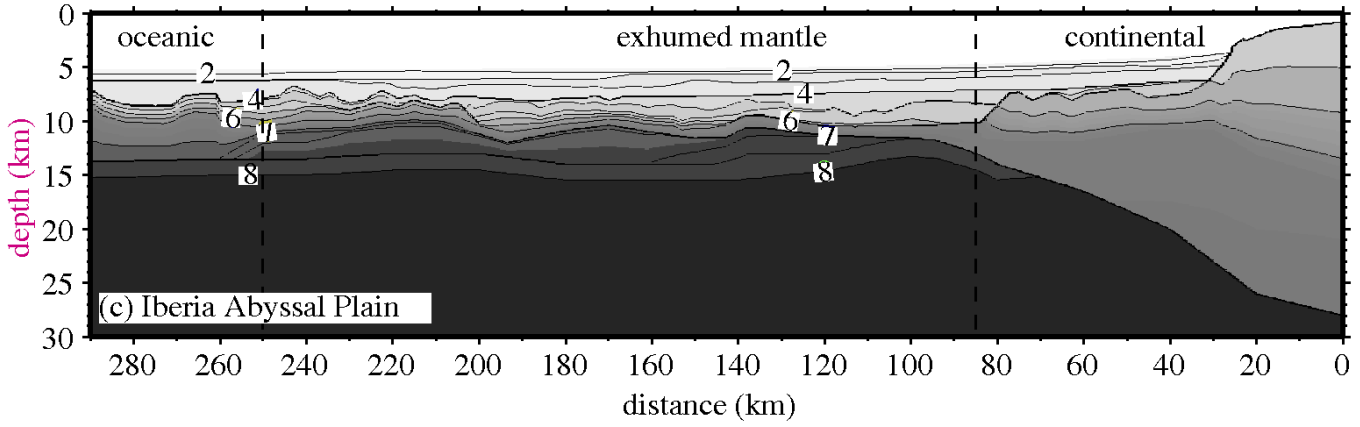


a) Hatton Bank



(b) Goban Spur





(a) Volcanic margin of Hatton Bank
Diagonal shading: seaward-dipping reflectors.
7.2 and 8.0 km s-1 region: magmatic rocks accreted to the base of the crust during rifting.
Transition from continental to oceanic crust occurs gradually between *ca*. 40 and 110 km.

b) Magma-poor Goban Spur margin.
Dashed line: inferred abrupt ocean-continent boundary.

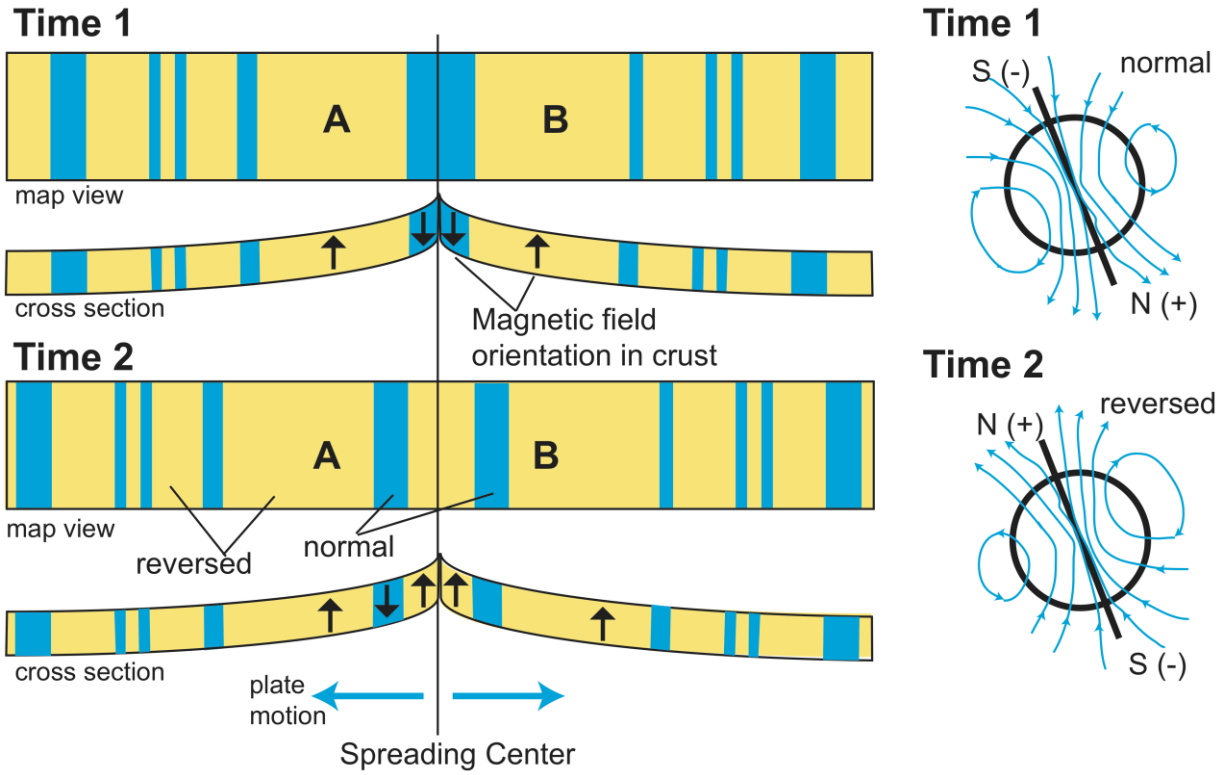
(c) West Iberia margin in the southern Iberia Abyssal Plain.
Dashed lines mark the approximate
edges of oceanic and of continental crust.

Minshull, 2002. The break-up of continents and the formation of new ocean basins. *Phil. Trans. R. Soc. Lond. A* 2002 **360**, 2839-2852

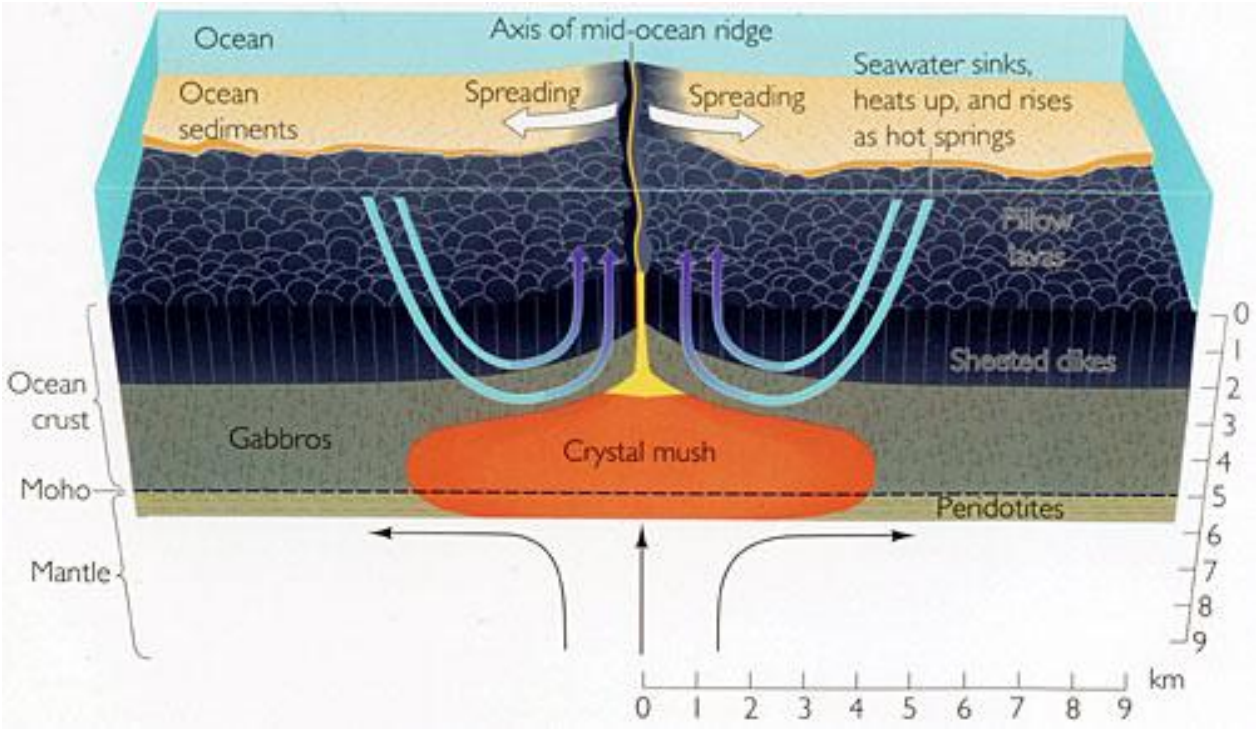
LITHOSPHERIC STRUCTURE INDICATORS

Magnetic anomalies

Certain minerals in the magma (e.g., magnetite) are sensitive to the Earth's magnetic field. As the magma cools, magnetic domains in these minerals will align with the Earth's magnetic field locking in the orientation (dip relative to horizontal) and polarity (field lines pointing out or field lines pointing in) of the magnetic field at that location.



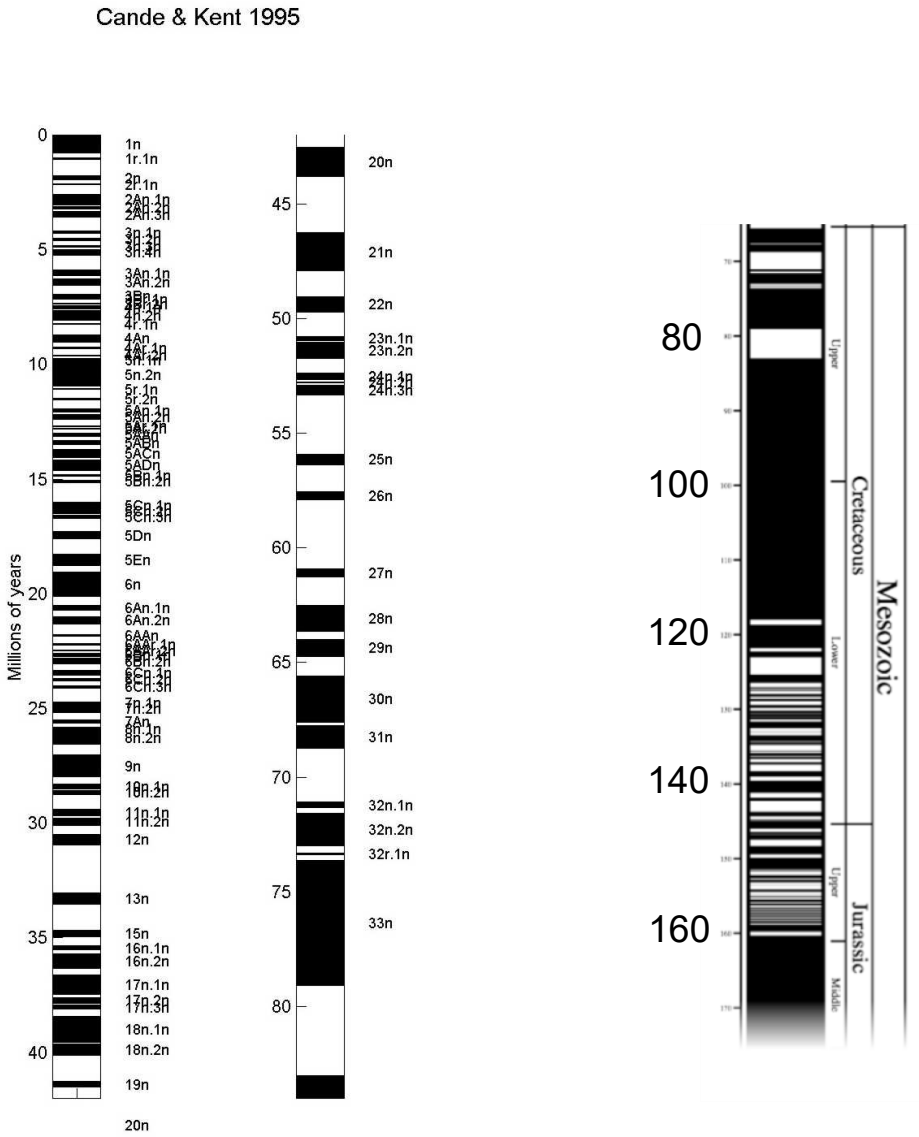
OCEANIC BASALTS RETAIN THE MAGNETIC ANOMALIES





OCEANIC SEDIMENTS RETAIN THE MAGNETIC ANOMALIES

Geomagnetic Polarity Time Scale (GPTS





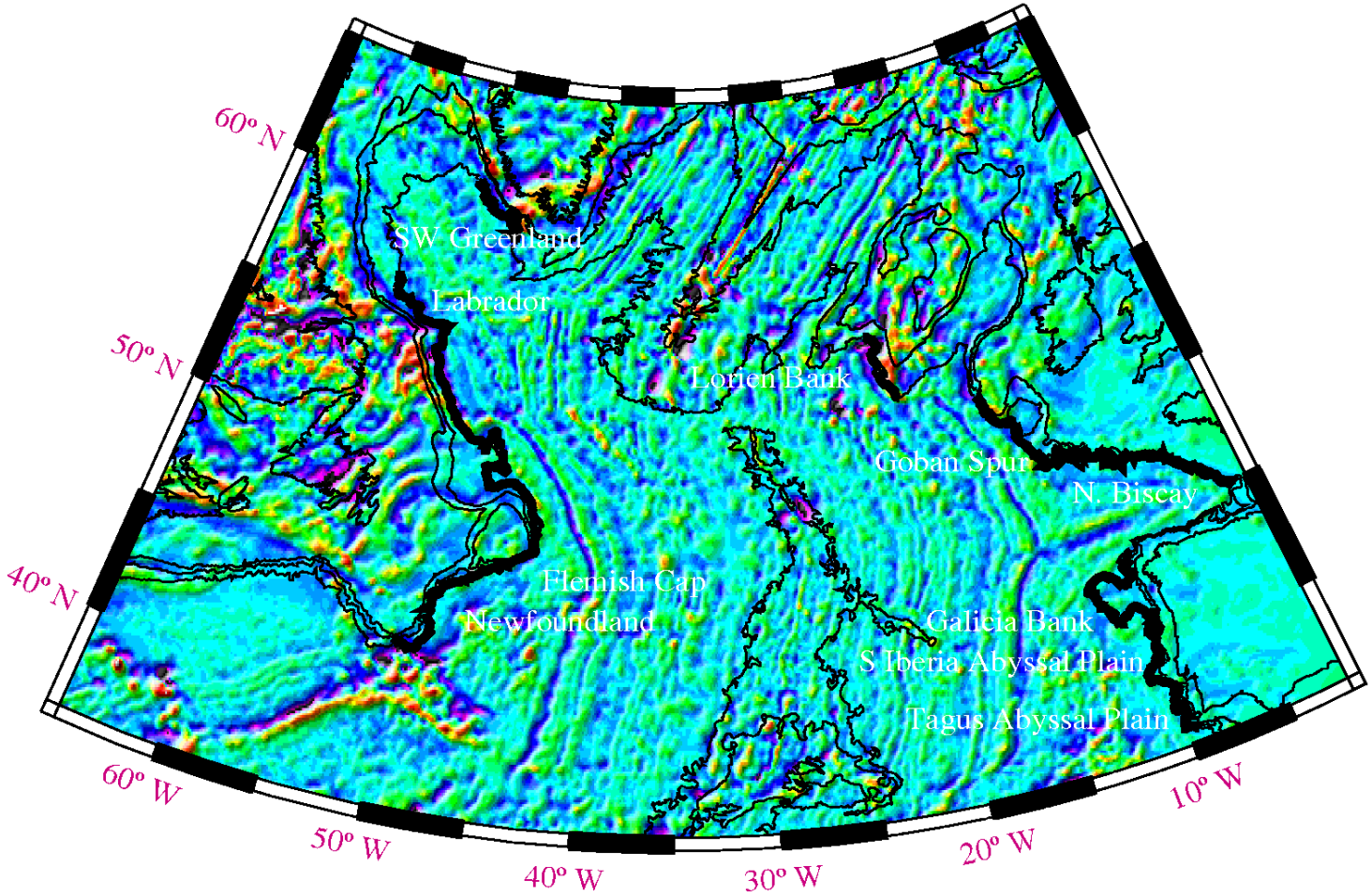
Instruments to measured the earth magnetic field in the ocean:

- Magnetometer

- gradiometer composed by two magnetometers to filter time variation in the magnetic field

Thick black lines mark magma-poor margins

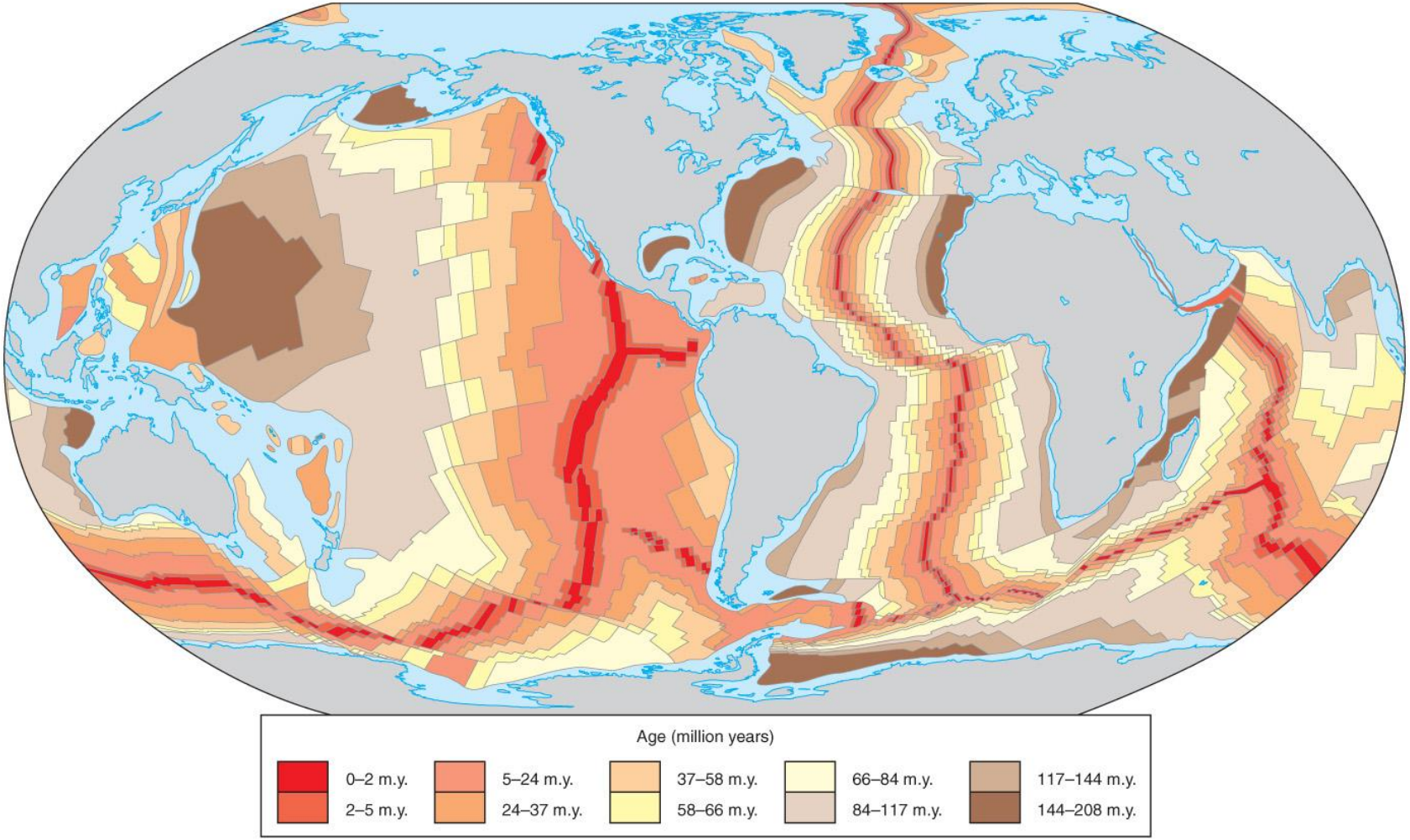
Linear magnetic anomalies appear close to the margins northwest of Scotland and southeast of Greenland
Large regions without such anomalies are present in the Bay of Biscay, west of Iberia and east of Newfoundland in the Labrador Sea



Minshull, 2002. The break-up of continents and the formation of new ocean basins. *Phil. Trans. R. Soc. Lond. A* 2002 **360**, 2839-2852

LITHOSPHERIC STRUCTURE INDICATORS

Magnetic anomalies



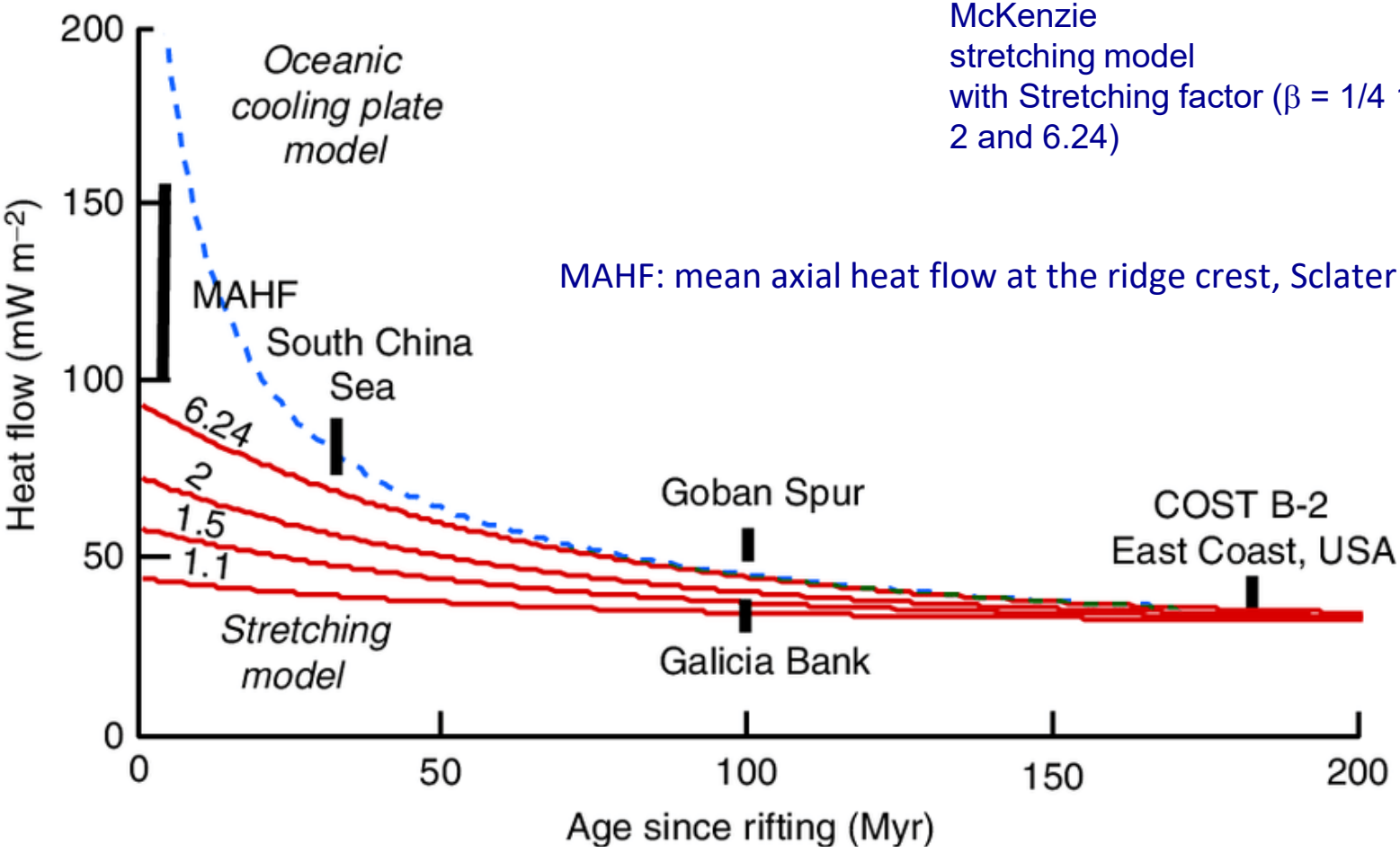
© 2011 Pearson Education, Inc.

LITHOSPHERIC STRUCTURE INDICATORS

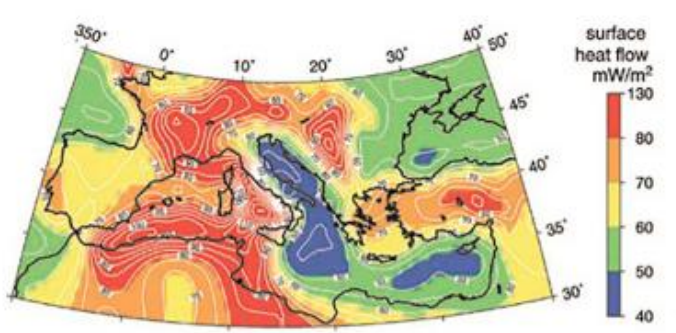
Heat Flow

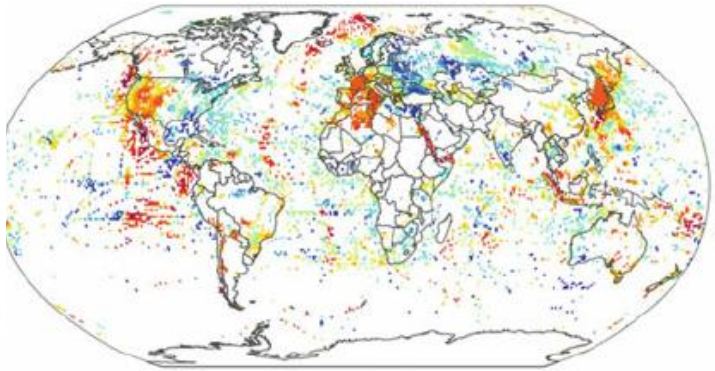
McKenzie
stretching model
with Stretching factor (β = 1/4 1.1, 1.5, 2 and 6.24)

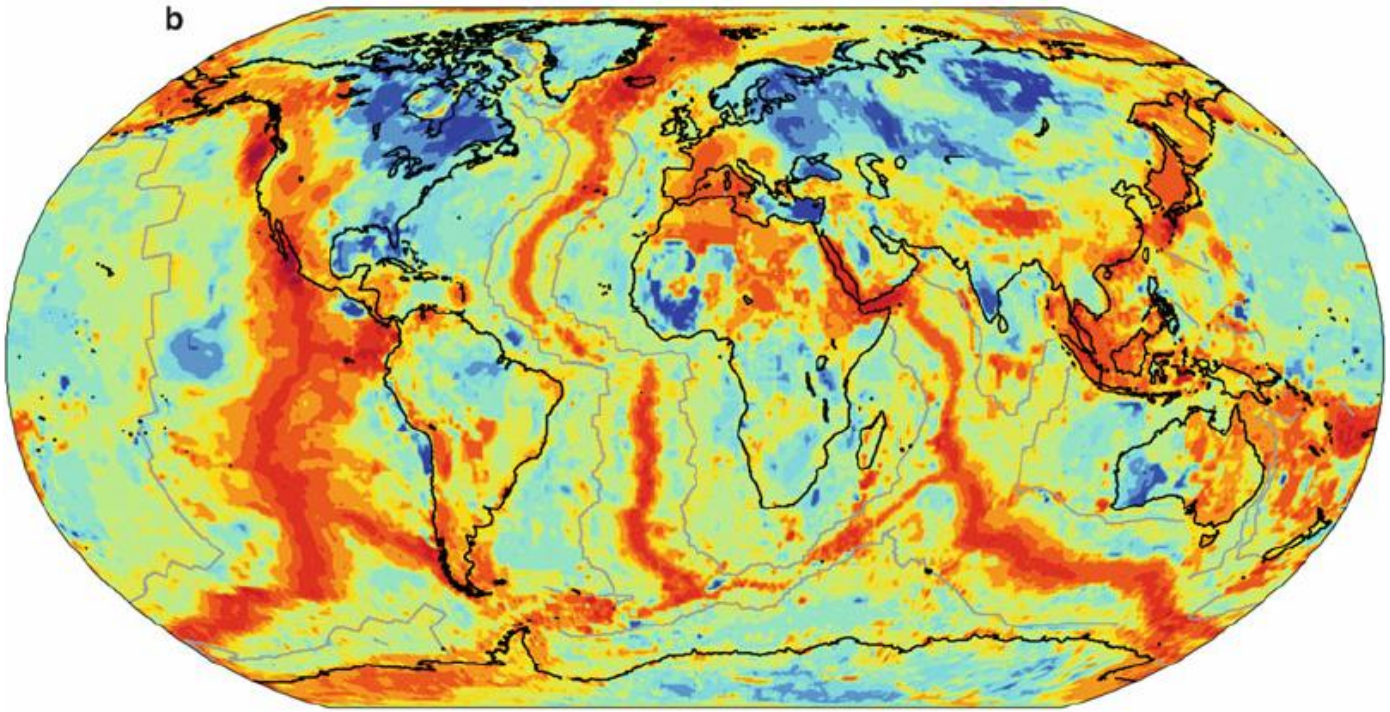
MAHF: mean axial heat flow at the ridge crest, Sclater et al. (1980)



Watts, 2012. Models for the evolution of passive margins. In Phanerozoic Rift Systems and Sedimentary Basins DOI:10.1016/B978-0-444-56356-9.00002-X







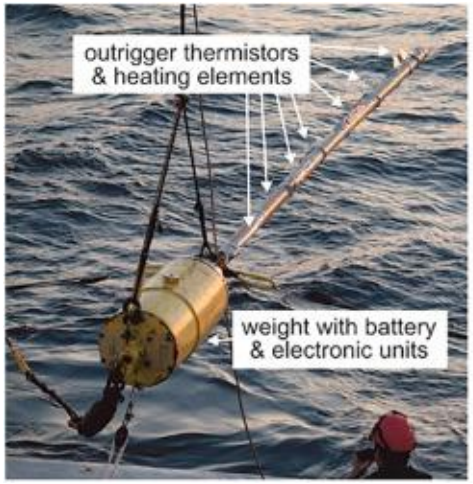
Goutorbe et al. (2011)
Global heat flow trends resolved from multiple geological and geophysical proxies. Geophysical Journal International, 187, 1405–1419.

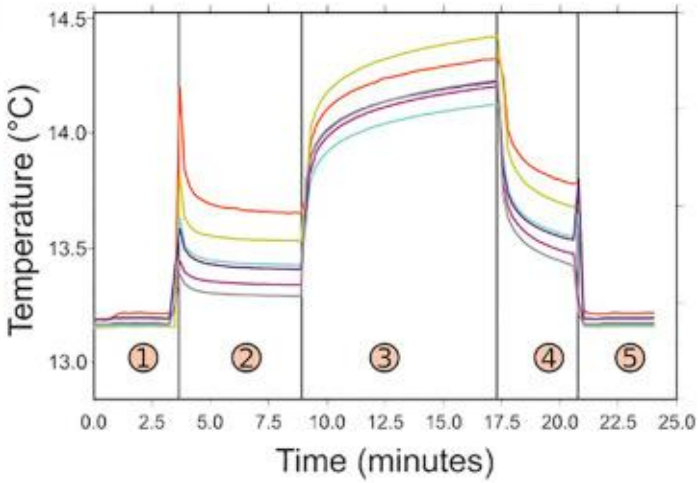
Mean heat flow (mW/m²)

<35 40 45 50 55 60 65 70 80 100 120 150 >200

Flusso di calore q = K *Δ**t**/Δ**z** (**mWxm**$^{-2}$)

K = conducibilità termica



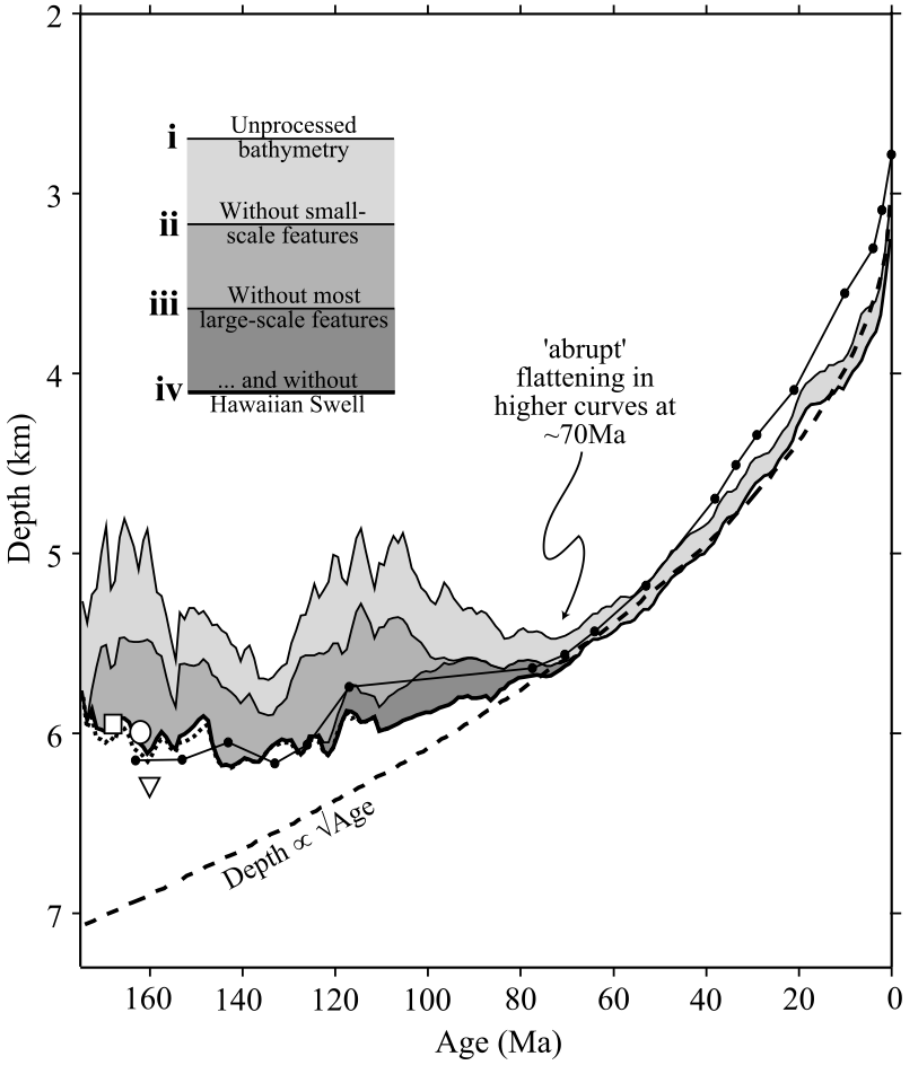


Poort et al., 2020. Heat flow in the Western Mediterranean: Thermal anomalies on the margins, the seafloor and the transfer zones. Marine Geology, Volume 419, 106064

LITHOSPHERIC STRUCTURE INDICATORS

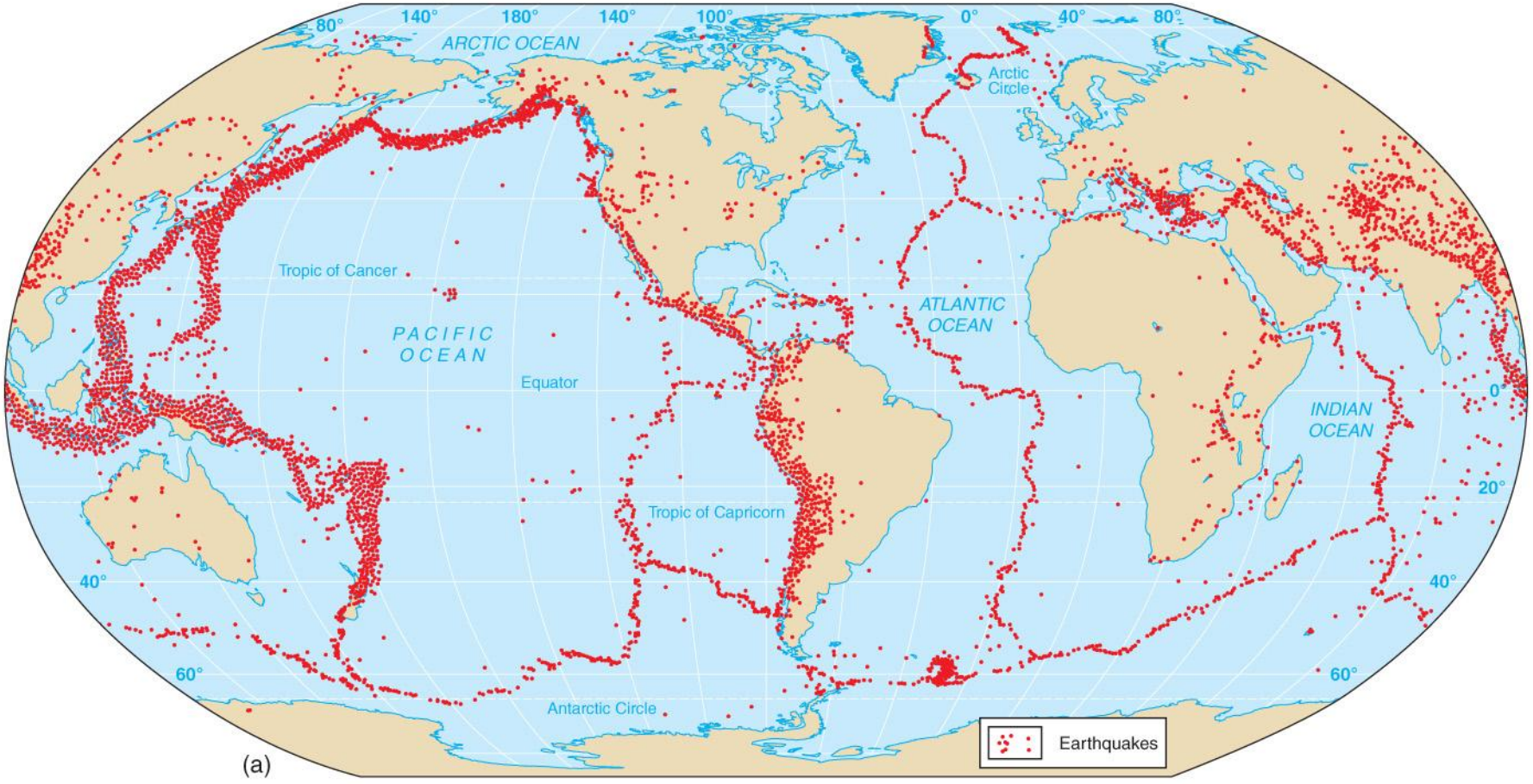
Age versus depth

Parsons and Sclater, 1977
Stein and Stein, 1992
Doin and Fleitout, 1996
Hillier and Watts, 2005



Hillier and Watts, 2005

PLATE BOUNDARIES



© 2011 Pearson Education, Inc.